Particle Plunges and Penrose Processes

Author: Conor Dyson

Niels Bohr Institute
Københavns Universitet

Supervisors: Vitor Cardoso and Maarten van de Meent

Abstract. This thesis is concerned with the exact dynamics of test particle motion in axisymmetric black hole spacetimes. The contents of this work can be largely divided into two halves, the first concerning itself with deriving analytic solutions to plunging geodesics in Kerr, in a form that can be implemented practically. The second half then explores the phenomenology of dyonic particles in Kerr-Newmann spacetimes. In the case of the Kerr solution, we derive closed-form solutions for the generic class of plunging geodesics in the extended geometry using Boyer-Lindquist coordinates. We also specialise to the case of test particles plunging from the innermost precessing stable circular orbit (ISSO) and unstable spherical orbits. We find these solutions in the form of elementary and Jacobi elliptic functions parameterised by Mino time. These solutions have been included in the `KerrGeodesics` package of the Black Hole Perturbation Toolkit as to be readily useful for application. In the latter half of this work, relating to Kerr-Newmann spacetimes, we analyse in depth the previously unstudied, modified Penrose process which can occur in magnetically charged spacetimes. Here we discover previously unseen, simply connected, ergoregions that are disconnected from the horizon. We also determine conditions on maximising these extended ergoregions given a fixed extremality. The content of this work is based on two pre-prints that were completed in the first half of 2023, namely, arXiv:2302.03704 and arXiv: 2306.15751, both of which are currently under peer-review.

Contents

Disclamer & Acknowledgements

The contents of this thesis are based on the arXiv pre-prints [1, 2] which were completed in collaboration with Maarten van de Meent and David Pereñiguez respectively. Unless otherwise stated, all novel results presented in this thesis are a consequence of calculations I completed explicitly whilst actively collaborating with the aforementioned researchers. I would like to thank both for their exceptional guidance in the first year of my integrated Masters/Ph.D. program. I would also like to thank Vitor Cardoso and Julie de Molade for their continued support throughout the integrated program. I acknowledge support from the Villum Investigator program supported by the VILLUM Foundation (grant no. VIL37766) and the DNRF Chair program (grant no. DNRF162) by the Danish National Research Foundation. This work makes use of the Black Hole Perturbation Toolkit [3].

1. Introduction

Analysing the geodesic structure of a spacetime is one of the foundational means of understanding strong field dynamics in an unperturbed state. This is apparent in the fact that the geodesics of the Kerr/Kerr-Newmann spacetimes have been extensively studied since their original derivations [4, 5]. Notably if one considers the coupling of gravitation to electromagnetism, described by the Einstein-Maxwell action, then the most general axisymmetric, asymptotically flat, stationary solution is given by the well-known Kerr-Newmann (KN) solution [4, 5]. The KN family of solutions contains four independent parameters, mass M, spin a, electric Q and magnetic P charges [6–9]. Notably in the limit $\{Q, P\} \to \{0, 0\}$, one smoothly recovers the Kerr metric. Most astrophysical black holes will be neutral. This is due to the fact that any accumulated charge on the hole is expected to be quickly neutralised by vacuum pair creation or interaction with the interstellar medium [10]. There are however well-known mechanisms, such as the Wald mechanism, whereby black holes immersed in constant magnetic fields can accrue a stable electric charge [11, 12], these charges are expected to be extremely small [13]. Given this, in most contexts, a physicist can have peace of mind in setting Q and P to zero when modeling astrophysical situations. This is how we shall proceed in the first half of this work. The intention here, to derive the analytic solutions to generic plunging geodesics in Kerr in support of current progress on perturbative calculations of two-body dynamics. This is not to say that dyonically charged black holes are uninteresting. KN black holes have captured the interest of theoretical astrophysicists for decades [14–19], and nowadays in the dawn of gravitational wave astronomy they play a prominent role in searches of beyond vacuum GR physics from ringdown analysis [20, 21], in modelling signatures of dark matter [22–32]. In addition, no known laws of physics prevent the existence of magnetic charges, and the incorporation of them into test particle motion in KN leads to rich and qualitatively new phenomena [1]. It is the responsibility of a theorist to explore these avenues and understand them to a full extent. This is the focus of the latter half of this work.

In solving analytically for generic timelike geodesics in Kerr. A critical step was the discovery of a fourth constant of motion, the Carter constant Q [33], which along with the mass shell condition, the conserved energy $\mathcal{E}$ and the angular momentum $\mathcal{L}$ allow for the full integrability of the geodesic equations of motion. Exact solutions for various special cases had been derived in the past [34, 35] no real effort was made to tackle the generic case until the start of the 21st century [36]. The introduction of the Mino time parameterisation [37] subsequently allowed for the full decoupling of the problem in a much simpler manner to previous approaches [33]. This opened the door for finding analytic solutions to generic bound geodesics in Kerr [38] as a system of piecewise smooth functions, which were then notably simplified through analytic continuation [39].

The full class of analytic solutions to Kerr-Newmann, Kerr-de Sitter and Kerr-anti-de Sitter space-times has been found generically [40, 41]. However, these solutions are presented in the form of Weierstrass elliptic and hyperelliptic Kleinian functions,

which can make them cumbersome to deal with. Recently, [42] has derived a much simplified analytic solution for the special case of equatorial plunging timelike geodesics which asymptote from the innermost stable circular orbit (ISCO). In this work, they also provide a simple expression for the equatorial radial inflow from the ISCO relevant to the study of accretion disk dynamics. In practice, these systems will not always be confined to the equatorial plane, motivating the generalisation of this result to the inclined (i.e. non-spin aligned or precessing) case, as we will do in this paper. In the interest of completeness, we also provide solutions for plunges starting from a general (inclined and eccentric) last stable orbit (LSO), i.e. asymptoting from a generic unstable spherical orbit (USO).

The work here on generic plunges is motivated by the role that geodesics play in the gravitational self-force approach to solving the relativistic dynamics of binary black holes [43]. In this approach, the dynamics are expanded in powers of the mass ratio between two black holes. In this scheme, the zeroth approximation to the motion of the lighter secondary component is given by a geodesic in the Kerr geometry generated by the (heavier) primary black hole. At higher orders, this motion is corrected by an effective force term, the gravitational self-force, causing the system to evolve. [44–46]. Consequently, the recent realisation that waveforms from the self-force formalism may be usable in the more comparable mass regime has led to a renewed interest in modeling the transition between bound and plunging motion of the secondary [47–53]. So far this effort has focused mostly on special cases involving quasi-circular (possibly precessing) inspirals. As the work progresses towards fully generic inspirals, there is a need for generic solutions for plunging geodesics. This work provides these by solving for completely generic closed-form analytic solutions for plunging geodesics in an easy-to-evaluate form.

Beyond analysing uncharged Kerr, the dyonically charged regime of KN provides a rich playground for understanding the qualitatively new dynamics which can occur in a simple, well-founded, extension to pure vacuum GR. One of the many reasons for interest in these systems is that charged black holes may play an important role in high-energy astrophysical phenomena such as cosmic rays [54], through an enhanced Penrose process. In charged KN, the enhancement of the Penrose process in the presence of an externally applied magnetic field (known as magnetised black holes) has been extensively studied for some time [55]. In practice, these magnetised systems can be quite difficult to model accurately and must be unphysically taken to exhibit a constant magnetic field at infinity. This presents multiple issues, one such being that magnetically charged black holes cannot be described in these setups (as they would lead to infinite accelerations on the hole). Additionally, these fields must either be regarded as test fields ignoring backreaction on the metric or lead to non-asymptotically flat solutions [56, 57]. Dyonically charged KN does not present these issues, acting as a completely well-defined asymptotically flat solution to the Einstein field equations. Much of the literature in the past has focused on charged black hole dynamics in the absence of magnetic charges. The primary motivation of the work in the latter part of this thesis

is to fill this gap and glean a concrete understanding of the qualitative differences which occur when one does not set the magnetic charge P to zero.

This thesis is outlined as follows, in section 2 we begin with an introduction to the Kerr-Newmann solution and the dyonic geodesic equations of motion, making manifest duality invariance. Using these quantities we will make explicit, definitions for the related conserved quantities. In section 4 we then restrict our attention to that of neutral particles in the Kerr spacetime. Here our attention will focus on the special cases of plunging timelike geodesics which asymptote from the innermost stable precessing circular orbit (ISSO) and plunges from unstable spherical orbits.‡ From these equations we determine the exact and two approximate expressions for the rate of radial inflow from the ISSO to the horizon. We then go on to determine the fully analytic solutions to these geodesic equations for ISSO plunges. In section 5 of this work, we go on to determine novel, fully analytic, expressions for generic timelike plunging geodesics in the Kerr spacetime in terms of elementary and (Jacobi) elliptic functions. These solutions to generic plunges are presented in a manifestly real form such to be easily implementable, supporting current work in the self-force community on the aforementioned transition to plunge. Following this, in section 6 we broadened our attention again to the full class of dyonically charged particle motion in KN. Here we derive the novel set of timelike geodesic in terms of elementary and Jacobi elliptic equations for bound and plunging motion. The motion of electric particles around electrically charged black holes has been extensively studied in the past. Given this, we restrict our attention to that of electric particles orbiting magnetic black holes. In particular, we find new necessary conditions for a particle to hit the singularity and show how the Carter constant loses its naive interpretation as a measure of orbital inclination in this set up. Additionally, we also show how these configurations lead to angular momentum being stored in the electromagnetic field and see how at extremality no geodesics crossing the horizon exist which would break cosmic censorship. Finally in section 7 we explore in depth the Penrose process in dyonically charged spacetimes. In particular, we discover previously unseen, simply connected ergoregions, which are disconnected from the horizon. We also determine conditions for maximising these extended ergoregions given a fixed extremality and show how in theory the efficiency of this process can become arbitrarily high. We work in geometric units where G = c = 1.

2. Kerr-Newmann and the Duality Invariant Equations of Motion

Kerr-Newmann is the most general, axisymmetric, asymptotically flat, stationary solution to Einstein-Maxwell action. The metric of this solution is given by the line

‡ In this paper, we use the acronym ISSO to refer to the general case of the last stable circular orbit for spherical (i.e. inclined precessing) orbits. The term ISCO will be used exclusively for the special case of circular equatorial last stable orbits.

element,

$$ds^2 = -\frac{\Delta - a^2\sin^2\theta}{\Sigma}dt^2 - 2a\sin^2\theta\left(\frac{r^2+a^2-\Delta}{\Sigma}\right)dtd\phi + \left(\frac{(r^2+a^2)^2 - \Delta a^2\sin^2\theta}{\Sigma}\right)\sin^2\theta d\phi^2 + \frac{\Sigma}{\Delta}dr^2 + \Sigma d\theta^2, \tag{1}$$

where

$$\Delta = r^2 - 2Mr + a^2 + Q^2 + P^2, \text{ and } \quad \Sigma = r^2 + a^2\cos^2\theta. \tag{2}$$

The corresponding Maxwell potential is given by,

$$A = -\frac{Qr}{\Sigma}\left(dt - a\sin^2\theta d\phi\right) + \frac{P\cos\theta}{\Sigma}\left(adt - (r^2+a^2)d\phi\right) . \tag{3}$$

With M and $a = J/M$ being the spacetimes ADM mass and Angular Momentum respectively. The quantities P and Q are the magnetic and electric charge of the spacetime defined by,

$$Q = \frac{1}{4\pi}\int_{S^2} \star F\,, \qquad P = \frac{1}{4\pi}\int_{S^2} F\,, \tag{4}$$

respectively, where S^2 is any surface of constant r §. Provided the condition $M^2 \geq a^2 + Q^2 + P^2$, the horizons of KN are given by,

$$r_\pm \coloneqq 1 \pm \sqrt{1 - a^2 - Q^2 - P^2}. \tag{5}$$

In stationary, analytic, asymptotically flat vacuum black hole spacetimes, $\mathcal{H}^+$(given by $r = rp$) is a Killing horizon [58]. In KN the killing vector associated with the outer horizon is given by,

$$k = \partial_t + \Omega_H\partial_\phi, \tag{6}$$

where $\Omega_H = a/(r_H^2 + a^2)$ is the angular velocity of the black hole as measured by an observer at infinity. Given a dyonically charged particle, that is a particle with both electric (e) and magnetic (g) charge the equations of motion for the particle in KN are given by,

$$u^a\nabla_a u_b = \frac{1}{m}\left(eF_{ba} - g\star F_{ba}\right)u^a\,. \tag{7}$$

The key step in understanding particle motion in these spacetimes is in general to then take Eqs 7 and express them as a system of decoupled first-order ODEs. This was firstly achieved by Carter [59] and later by others [40, 60]. Here we will begin by outlining an alternative derivation of this decoupled equation which keeps all quantities manifestly duality invariant.

In the dyonic KN one finds an explicit symmetry arises in the field equations, known as electric-magnetic duality. This symmetry corresponds to rotations between electric and magnetic charges by $S^I{}_J \in SO(2)$ and can be thought of as a fundamental property

§ Here $\star F$ is the Hodge dual of the Maxwell tensor given in components as, $\star F_{ab} \coloneqq \frac{1}{2!}\epsilon_{abcd}F^{cd}$, with ϵ_{abcd} being the volume form of the manifold.

of Einstein-Maxwell theory. Here we make this symmetry explicit by re-writing the equations in terms of duality invariant quantities. We first begin by collecting certain electric-magnetic quantities into two-component vectors,

$$F^I = \begin{pmatrix} F \\ \star F \end{pmatrix}, \; Q^I = \begin{pmatrix} P \\ Q \end{pmatrix}, \; q^I = \begin{pmatrix} g \\ e \end{pmatrix}, \qquad (I = 1, 2)\,, \tag{8}$$

and introduce the euclidean and symplectic metrics

$$\delta_{IJ} = \begin{pmatrix} 1 & 0 \\ 0 & 1 \end{pmatrix}, \qquad \Omega_{IJ} = \begin{pmatrix} 0 & 1 \\ -1 & 0 \end{pmatrix}, \tag{9}$$

which are the generators of the infinitesimal symmetry group of $S^I{}_J \in SO(2)$. Under these transformations the metrics (9) remain invariant, that is,

$$\delta_{IJ} = S^K{}_I S^L{}_J \delta_{KL}\,, \qquad \Omega_{IJ} = S^K{}_I S^L{}_J \Omega_{KL}\,. \tag{10}$$

Defining these invariant quantities the equations of motion (7) now take the form,

$$u^a \nabla_a u_b = \frac{1}{m} \Omega_{IJ} F^I_{ba} q^J u^a \tag{11}$$

which is manifestly duality invariant. In order to reduce the above system of second-order ODEs in terms of first-order ODEs we must re-write the equations of motion in terms of quantities conserved along the trajectories governed by 11. Taking, $\mathcal{P}^I_\xi = (\mathcal{P}_\xi, \tilde{\mathcal{P}}_\xi)$, to be the duality vector given by ξ. Defined such that the components of $\mathcal{P}^I_\xi$ can be found explicitly through the equation,

$$\nabla_a \mathcal{P}^I_\xi = -\xi^b F^I_{ba}\,. \tag{12}$$

Then if ξ is a Killing vector of the background which also leaves the Maxwell tensor invariant we can construct a conserved quantity by,

$$C_\xi = u_a \xi^a + \frac{1}{m} \Omega_{IJ} \mathcal{P}^I_\xi q^J. \tag{13}$$

Taking the boundary conditions to be given by $\int_{S^2_\infty} \mathcal{P}^I_\xi d\Omega = 0$ then $\mathcal{P}_X$ and $\tilde{\mathcal{P}}_X$ directly correspond to the electric and magnetic momentum maps of ξ in line with the terminology of [61–63]. In particular, taking $\xi = k$ (the generator of the outer Killing horizon) and evaluating on $\mathcal{H}^+$ these quantities become precisely the electromagnetic potentials of the black hole.

Additional constants of motion can also exist if the spacetime admits a Stackel-Killing tensor $K_{\mu\nu}$ [59, 64], defined to satisfy,

$$K_{ab} = K_{ba}\,, \quad \nabla_{(a} K_{bc)} = 0\,, \tag{14}$$

the standard Killing tensor conditions, along with the additional algebraic constraints,

$$K_{c(a} F_{b)}{}^c = 0\,, \quad K_{c(a} \star F_{b)}{}^c = 0 \tag{15}$$

which are required in the presence of the additional Maxwell fields. If such a tensor exists, then

$$C = K_{ab}u^a u^b, \tag{16}$$

gives as a further conserved quantity. Often left unmentioned is that the metric satisfies this Killing-Stackle condition, giving rise to the usual mass shell condition for a test particle.

The time ∂_t and azimuthal ∂_ϕ Killing vectors and their associated duality vectors, give rise to two constants of motion through 13. With the electric momentum maps of the Killing vectors given by,

$$\mathcal{P}_t(P,Q) = -\frac{Qr - Pa\cos\theta}{\Sigma}\,, \text{ and} \tag{17}$$

$$\mathcal{P}_\phi(P,Q) = \frac{Qar\sin^2\theta - (a^2+r^2)\,P\cos\theta}{\Sigma}. \tag{18}$$

The associated magnetic momentum maps are then found through the simple relations, $\tilde{\mathcal{P}}_t(P,Q) = \mathcal{P}_t(Q,-P)$ and $\tilde{\mathcal{P}}_\phi(P,Q) = \mathcal{P}_\phi(Q,-P)$. The calculation of these momentum maps in an explicitly duality invariant manner was primarily the work of my collaborator David Pereñiguez. Finally one can also determine a Carter-like constant in Dyonic KN spacetimes through the existence of the non-trivial Stackle-Killing tensor[59, 65, 66],

$$\mathcal{K}_{ab} = 2\Sigma l_{(a}n_{b)} + r^2 g_{ab}\,. \tag{19}$$

Where

$$l = \frac{r^2+a^2}{\Delta}\partial_t + \partial_r + \frac{a}{\Delta}\partial_\phi\,, \text{ and} \tag{20}$$

$$n = \frac{1}{2\Sigma}\left[(r^2+a^2)\partial_t - \Delta\partial_r + a\partial_\phi\right] \tag{21}$$

are the principal null directions of the Kinnersly tetrad [67]. These constants of motion can then be found explicitly as ‖,

$$\begin{aligned}\mathcal{E} &\equiv -u_a\,(\partial_t)^a - \frac{1}{m}\Omega_{IJ}\mathcal{P}_t^I q^J \\ &= -u_a\,(\partial_t)^a + \frac{r\delta - a\Omega\cos\theta}{m\Sigma}\,,\end{aligned} \tag{22}$$

$$\begin{aligned}\mathcal{L} &\equiv u_a\,(\partial_\phi)^a + \frac{1}{m}\Omega_{IJ}\mathcal{P}_\phi^I q^J \\ &= u_a\,(\partial_\phi)^a + \frac{ar\delta\sin^2\theta - \Omega(r^2+a^2)\cos\theta}{m\Sigma}\,,\end{aligned} \tag{23}$$

$$\mathcal{K} \equiv u^a u^b \mathcal{K}_{ab} - (\mathcal{L} - a\mathcal{E})^2 \tag{24}$$

$$m \equiv -u^a u^b g_{ab}\,. \tag{25}$$

‖ One is always free to shift these conserved quantities by any constant value they wish. Here we elect to choose a constant shift in $\mathcal{K}$ of $(\mathcal{L}-a\mathcal{E})^2$. This is a common choice in Kerr as it is this shifted quantity that gives precisely equatorial orbits when zero. We make the same choice in dyonic KN for the sake of consistency and to later make explicit some subtle differences that arise in this quantity in dyonic KN from Kerr.

Where here we have defined the duality invariant quantities,

$$\delta = \delta_{IJ} Q^I q^J = Qe + Pg\,, \qquad \text{and} \qquad \Omega = \Omega_{IJ} Q^I q^J = Pe - Qg\,. \tag{26}$$

Here the δ term can be thought of as a measure of "electric-electric" interaction whereas Ω can be thought of as a measure of "Magnetic-electric" interaction. Then, inverting the relations for the conserved quantities, using the Mino–Carter time $d\tau = \Sigma d\lambda$ [37] as a curve parameter and introducing $z = \cos\theta$, the equations of motion can be decoupled and cast in the form

$$\begin{aligned}\left(\frac{dr}{d\lambda}\right)^2 =& \frac{\left(m(\mathcal{E}(r^2+a^2) - a\mathcal{L}) - r\delta\right)^2}{m^2} - \Delta(r^2 + (a\mathcal{E} - \mathcal{L})^2 + \mathcal{K}) \\ \equiv& R(r)\,,\end{aligned} \tag{27}$$

$$\begin{aligned}\left(\frac{dz}{d\lambda}\right)^2 =& \mathcal{K} - z^2\mathcal{K} - \frac{z^2(\Omega^2 + m^2\mathcal{L}^2) + 2m\Omega\mathcal{L}z}{m^2} + az(1-z^2)\frac{2\mathcal{E}\Omega - amz(1-\mathcal{E}^2)}{m} \\ \equiv& Z(z)\,,\end{aligned} \tag{28}$$

$$\frac{d\phi}{d\lambda} = \frac{\Omega z + m(\mathcal{L} - a\mathcal{E}(1-z^2))}{m(1-z^2)} - \frac{a}{m\Delta}(\delta r + am\mathcal{L} - m(a^2+r^2)\mathcal{E})\,, \tag{29}$$

$$\frac{dt}{d\lambda} = (a^2+r^2)\frac{m(a^2+r^2)\mathcal{E} - am\mathcal{L} - \delta r}{m\Delta} + a\frac{m(\mathcal{L} - a\mathcal{E}(1-z^2)) + \Omega z}{m}\,. \tag{30}$$

3. Plunging Motion in Kerr

Sections 3, 4 and 5 of this thesis will be concerned with plunging motion in Kerr, hence with the exception of section 7 we set the quantities $\{e, q, P, Q\} = \{0, 0, 0, 0\}$. In particular, this reduces the geodesic equations of motion to the form, [33],

$$\begin{aligned}\left(\frac{dr}{d\lambda}\right)^2 &= (\mathcal{E}(r^2+a^2) - a\mathcal{L})^2 - \Delta(r^2 + (a\mathcal{E} - \mathcal{L})^2 + \mathcal{K}) \\ &= (1-\mathcal{E}^2)(r_1 - r)(r_2 - r)(r_3 - r)(r - r_4) \\ &\equiv R(r),\end{aligned} \tag{31}$$

$$\begin{aligned}\left(\frac{dz}{d\lambda}\right)^2 &= \mathcal{K} - z^2(a^2(1-\mathcal{E}^2)(1-z^2) + \mathcal{L}^2 + \mathcal{K}) \\ &= (z^2 - z_1^2)(a^2(1-\mathcal{E}^2)z^2 - z_2^2) \\ &\equiv Z(z),\end{aligned} \tag{32}$$

$$\frac{dt}{d\lambda} = \frac{(r^2+a^2)}{\Delta}(\mathcal{E}(r^2+a^2) - a\mathcal{L}) - a^2\mathcal{E}(1-z^2) + a\mathcal{L}\,, \tag{33}$$

$$\frac{d\phi}{d\lambda} = \frac{a}{\Delta}(\mathcal{E}(r^2+a^2) - a\mathcal{L}) + \frac{\mathcal{L}}{1-z^2} - a\mathcal{E}, \tag{34}$$

where, now in the absence of external forces, due to the equivalence principle we can take $m = 1$ without loss of generality. By taking advantage of the Mino time parameterisation the equations of motion completely decouple and can be solved hierarchically. This is done by first solving for $r(\lambda)$ and $z(\lambda)$ then naturally solving the equations in the form $t(r, z, \lambda) = t_r(r) + t_z(z) - a\mathcal{E}\lambda$ and $\phi(r, z, \lambda) = \phi_r(r) + \phi_z(z) + a\mathcal{L}\lambda$. The solutions for $r(\lambda)$ and $z(\lambda)$ can be directly substituted to obtain $t(\lambda)$ and $\phi(\lambda)$.

Analysing the radial equation in its explicit form (31), one can see that the distinction between bound and plunging orbits is fully determined by the root structure of the fourth-order polynomial $R(r)$. In particular, plunges occur when we have bound motion between some roots r_i, r_j of $R(r)$ with $r_i < r_- < r_+ < r_j$. In this work, we restrict to geodesics with $\mathcal{E} < 1$, which implies that the radial potential $R(r)$ is negative in the limit $r \to \infty$, ensuring that the geodesic is bound to the Kerr black hole. Moreover, since $R(r_\pm) > 0$ it guarantees that there is at least one real root of $R(r)$ outside r_+. A less obvious implication comes from the polar equation (32). Rewriting the polar potential as

$$Z(z) = (1 - z^2)\,\mathcal{K} - z^2(a^2(1 - \mathcal{E}^2)(1 - z^2) + \mathcal{L}^2), \tag{35}$$

it becomes apparent that when $\mathcal{E} < 1$ the polar equation has solutions with $-1 < z < 1$ if and only if $\mathcal{K} \geq 0$. For the radial potential, this implies that $R(0) \leq 0$, and consequently that there exists at least one real root of the radial equation between $r = 0$ and the inner horizon. We thus find that for any values of $\mathcal{E} < 1$ and $\mathcal{K} \geq 0$, there exists a plunging geodesic. It is important to note that the case of $\mathcal{E} > 1$ with $\mathcal{K} < 0$ also contributes to a small subset of parameter space for which a real solution is allowed. Its dynamics are quite interesting as by a brief analysis of the equations of motion one can see that this would give a test particle which plunges from infinity, poloidally oscillating around some $z_0 \neq 0$.

Generically, a plunging geodesic will eternally oscillate between two turning points of the radial potential and return to the same radial point after a finite amount of Mino (and proper) time. Geometrically, this corresponds to a geodesic diving into the Kerr black hole and passing through the two horizons before being scattered back out, passing the horizons in reversed order and exiting in a different asymptotically flat region of the maximally extended Kerr solution, as shown in the Penrose diagrams in Fig. 1.

Exceptions to this picture occur for equatorial trajectories and when one of the bounding roots has a multiplicity greater than one. In the first case $\mathcal{K} = 0$, one finds that $r = 0$ is a root of the radial equation. If this is the inner turning point of the geodesic, the plunge will end on the singularity after a finite amount of Mino (and proper) time. In the second case, approaching a root with higher multiplicity takes an infinite amount of Mino (and proper) time. In Section 4, we will see the physically relevant case where the outer turning point of the solution is a triple root, i.e. lies on the ISSO, where the radial solution takes a particularly simple form generalising the result of [42]. The right panel in Fig. 1 shows this edge case trajectory in a Penrose diagram.

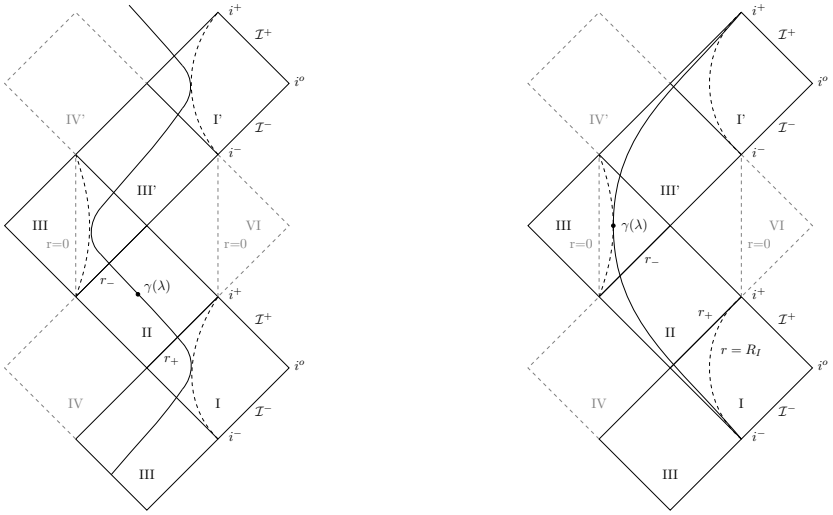

Figure 1. Penrose diagrams of the maximally analytic extension of the Kerr metric showing different plunge trajectories. Left Image: A generic plunging orbit whereby the solutions oscillate between the largest root of $R(r)$ which is less than r_- and the smallest root of $R(r)$ greater than r_+. These trajectories correspond to geodesic motion entering the black hole, reaching a turning a point, and exiting the white hole into a different asymptotically flat region. Each point on the dashed lines in region I and I' correspond to a spacelike 2-surface of constant radius corresponding to the outer turning point. Right Image: A plunge which asymptotes to r_I as $\lambda \to \pm\infty$, where $\gamma(\lambda)$ represents the geodesic in question. On the Penrose diagram, these trajectories begin at past spacial infinity i^- and end at future spacial infinity i^+ in a different asymptotically flat region. Each point on the dashed lines in region I and I' correspond to a spacelike 2-surface of constant radius corresponding to the ISSO radius r_I

In the generic case, we know at least two of the four roots of $R(r)$ are real. The other two roots are either both real or both complex. If the other two roots are real, they come in a pair that lies either entirely outside the outer turning point, entirely between the inner turning point and $r = 0$, or entirely in the $r < 0$ region. In the first of these cases, the plunging orbit exists inside of a normal bound orbit, a case sometimes referred to as a "deeply bound" orbit. The solutions for cases with 4 real roots turn out to be a straightforward generalisation from the solutions of [38, 39]. The derivation of the solution for the complex case will turn out to be substantially more involved.

4. The Innermost Precessing Stable Circular Orbit in Kerr

Before determining the solutions to fully generic plunges in Kerr we begin by solving for plunges which asymptote to the ISSO. In this case the radial potential $R(r)$ is imbued with a triple root at the ISSO radius $r = r_I$. Two of these roots come from the fact that the ISSO must be a (precessing) circular orbit and the additional root arises from the fact we are looking specifically at the innermost of these orbits meaning $R(r)$ must

also inflect at this point. As a result, we determine a radial equation of the form

$$\left(\frac{dr}{d\lambda}\right)^2 = (1-\mathcal{E}^2)(r_I - r)^3(r - r_4). \tag{36}$$

By equating Eq. (31) with Eq. (36) one immediately obtains the result,

$$r_4 = \frac{a^2\,\mathcal{K}}{(1-\mathcal{E}^2)r_I^3}. \tag{37}$$

The roots of the polar equation can be found to be given by [68],

$$z_1 = \sqrt{\frac{1}{2}\left(1 + \frac{\mathcal{L}^2+\mathcal{K}}{a^2(1-\mathcal{E}^2)} - \sqrt{\left(1+\frac{\mathcal{L}^2+\mathcal{K}}{a^2(1-\mathcal{E}^2)}\right)^2 - \frac{4\,\mathcal{K}}{a^2(1-\mathcal{E}^2)}}\right)}, \text{ and} \tag{38a}$$

$$z_2 = \sqrt{\frac{a^2(1-\mathcal{E}^2)}{2}\left(1 + \frac{\mathcal{L}^2+\mathcal{K}}{a^2(1-\mathcal{E}^2)} + \sqrt{\left(1+\frac{\mathcal{L}^2+\mathcal{K}}{a^2(1-\mathcal{E}^2)}\right)^2 - \frac{4\,\mathcal{K}}{a^2(1-\mathcal{E}^2)}}\right)}. \tag{38b}$$

Finally, we define

$$k_z = a\sqrt{(1-\mathcal{E}^2)}\frac{z_1}{z_2}, \tag{39}$$

as a quantity which will recurrently show up throughout this work.¶

Naturally, geodesics asymptoting to the ISSO must also share the same constants of motion as the ISSO. We can therefore identify a plunging geodesic of this type with those of a particular ISSO, which has two degrees of freedom. These two degrees of freedom can be set by picking a black hole spin (a) and maximum orbital angle of inclination $\theta_{max} \in (-\frac{\pi}{2}, \frac{\pi}{2})$. This then determines a unique r_I. One can also invert this relation to set the parameterisation in terms of (a, r_I). Making this choice one finds for each value of a there exists a range of allowed r_I's each of which corresponds to a unique inclination either in prograde or retrograde. The innermost and outermost of these quantities correspond to the equatorial ISCOs in prograde and retrograde respectively. Defining $A = (27 - 45a^2 + 17a^4 + a^6 + 8a^3(1-a^2))^{\frac{1}{3}}$ and $B = \sqrt{3 + a^2 + \frac{9-10a^2+a^4}{A} + A}$ the range of possible r_I values for a given a are,

$$R_{I,\text{min/max}} = 3 + B \mp \frac{1}{2}\sqrt{\left(72 + 8(a^2-6) - \frac{4(9-10a^2+a^4)}{A} - 4A + \frac{64a^2}{B}\right)}. \tag{40}$$

Forms of these bounds have been known in the literature for some time [69]. If one wishes to parameterise by inclination, one can use the `KerrGeodesics` package in the Black hole perturbation theory toolkit [3] to find $\mathcal{E}, \mathcal{L}$ and $\mathcal{K}$ parameterised by (a, θ_{inc}), where θ_{inc} runs from 0 for equatorial prograde orbits to π for equatorial retrograde orbits [70].

¶ Note that the definition of k_z (and later k_r) differs from the conventions used in [39].

In parameterising the conserved quantities by (a, r_I) we begin with the expression for the marginally stable spherical orbits $\mathcal{K}$ written in terms of r_I [71] which gives,

$$\mathcal{K} = r_I^{\frac{5}{2}} \frac{(\sqrt{(r_I - r_+)(r_I - r_-)} - 2\sqrt{r_I})^2 - 4a^2}{4a^2(\sqrt{(r_I - r_+)(r_I - r_-)} + \sqrt{r_I} - r_I^{\frac{3}{2}})}. \tag{41}$$

Equating the remaining coefficients between Eq. (31) and Eq. (36) we obtain the equations,

$$\mathcal{E} = \frac{\sqrt{a^2\,\mathcal{K} - 2r_I^3 + 3r_I^4}}{\sqrt{3}r_I^2}, \quad \text{and} \tag{42}$$

$$\mathcal{L} = \pm \frac{\sqrt{3a^2\,\mathcal{K} - a^2 r_I^2 - {}_I^2 + 3r_I^4 + a^2 r_I^2 \mathcal{E}^2 - 3r_I^4 \mathcal{E}^2}}{r_I}. \tag{43}$$

Where the $\pm$ is determined by whether or not the r_I picked corresponds to a prograde or retrograde orbit respectively. The correct sign is determined by the condition,

$$\text{Sign} = \begin{cases} +, & \text{if } r_I \leq \mathcal{L}_{\text{root}} \\ -, & \text{if } r_I > \mathcal{L}_{\text{root}} \end{cases}, \tag{44}$$

where, defining $\kappa = \sqrt{a^2 - 2r + r^2}$, the value of $\mathcal{L}_{\text{root}}$ is given as the root of the function

$$\begin{aligned} \alpha(r) = a^6 - 3a^2 r^{\frac{5}{2}}(3r^{\frac{3}{2}} + \kappa(6 - 2r)) + r^{\frac{9}{2}}(r^{\frac{1}{2}}(20 - 11r) + \kappa(5 + 3r)) \\ + a^4(r(3r - 4) + \kappa r^{\frac{1}{2}}(1 + 3r)), \end{aligned} \tag{45}$$

which is real and closest to $r = 6$. Eq. (45) has been given in a form such that the root can be found numerically to high precision which is not the case for Eq. (43). It is worth noting that as $\mathcal{E}, \mathcal{L}$, and $\mathcal{K}$ have all been determined in terms of r_I, and z_1 is the root that defines the maximum range of oscillation allowed for a given r_I, our solution immediately defines a spacelike surface $(r, z, \phi) = (r_I, z_1(r_I), u)$ for $r_I \in (r_{Imin}, \mathcal{L}_{\text{root}})$ and $u \in (0, 2\pi)$ inside which no stable spherical orbits can exist. Taking our exact solution for this spacelike surface to the extremal limit also provides us with the ISSO surfaces found in the near-horizon extremal Kerr geometry previously found in both [72] and [73].

We are now ready to begin analysing the physical consequences of extending the results of [42], regarding equatorial ISCO flow to inclined orbits. The exact solution to this equation includes functional dependence on certain Jacobi elliptic functions. In order to simplify the results we provide two approximate forms of the inflow. The first, approximated to a modified form of the equatorial inflow equation which removes all dependence on Jacobi elliptic functions. The second, a polar averaged form which simplifies the functional dependence on the Jacobi elliptic functions to a constant dependence for any given set of parameter values. We find the modified equatorial flow to be given by,

$$\left.\frac{dr}{dt}\right|_{\text{Equatorial}} = \frac{-\sqrt{(1 - \mathcal{E}^2)(r_I - r)^3(r - \frac{a^2\,\mathcal{K}}{(1-\mathcal{E}^2)r_I^3})}}{a\mathcal{L} + \frac{(r^2+a^2)}{\Delta}(\mathcal{E}(r^2 + a^2) - a\mathcal{L}) - a^2\mathcal{E}}. \tag{46}$$

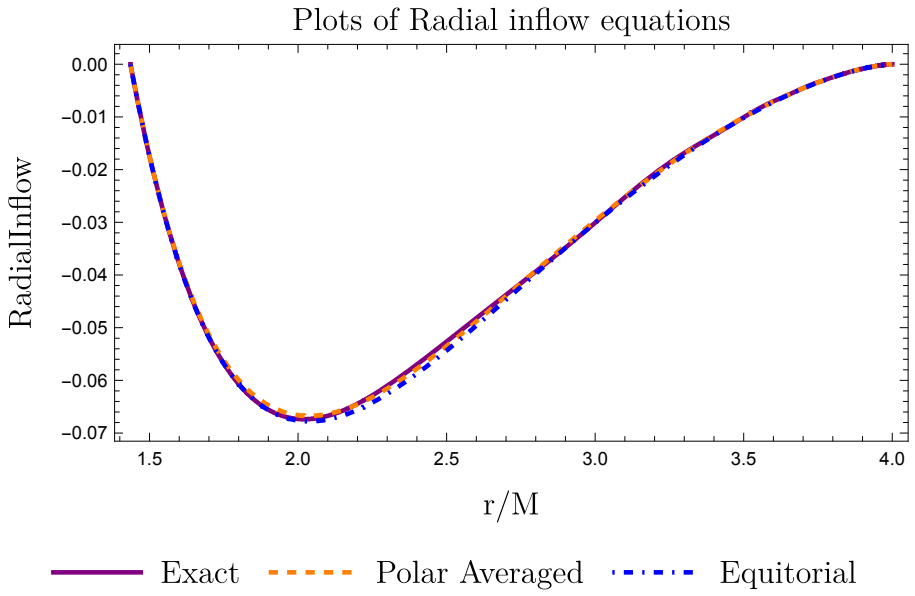

Figure 2. Plot of differing radial inflow equations from the ISSO to horizon, for parameter values (a, r_I) =(0.9,4) for plot range (r_+, r_I) on the radial axis. The lightly oscillating purple line corresponds to the exact solution exhibiting small oscillations over each polar period. The blue and orange dashed lines correspond to the equatorial and polar averaged approximations respectively. The Radial flow measured on the y-axis is given by the dimensionless quantity dr/dt for each of the three flow equations.

In the equatorial limit ($\mathcal{K} = 0$), this reproduces the result of [42], but gives an improved representation of the radial inflow for inclined disks where Q, $\mathcal{E}$,and $\mathcal{L}$ are given by their true values Eqs. (41),(42) and (43) respectively. Next, we go on to determine the form of the radial inflow when averaged over the polar period, this is found to be

$$\left.\frac{dr}{d\langle t\rangle_z}\right|_{\text{PolarAvg}} = \frac{-\sqrt{(1-\mathcal{E}^2)(r_I-r)^3(r-\frac{a^2\mathcal{K}}{(1-\mathcal{E}^2)r_I^3})}}{a\mathcal{L}+\frac{(r^2+a^2)}{\Delta}(\mathcal{E}(r^2+a^2)-a\mathcal{L})-a^2\mathcal{E}+\frac{z_2^2\mathcal{E}}{1-\mathcal{E}^2}\left(1-\frac{\mathsf{E}(k_z^2)}{\mathsf{K}(k_z^2)}\right)}. \tag{47}$$

Where $\mathsf{K}(\cdot)$ and $\mathsf{E}(\cdot)$ are the complete elliptic functions of the first and second kind respectively. We have defined the polar average as follows, given some function $f(\lambda)$ that (partially) depends on λ through z such that $f(\lambda) = F(r(\lambda), z(\lambda), \lambda)$, we take

$$\langle f\rangle_z(\lambda) = \frac{1}{\Lambda_z}\int_{-\Lambda_z/2}^{\Lambda_z/2} F(r(\lambda), z(\lambda+\delta), \lambda)d\delta, \tag{48}$$

where

$$\Lambda_z = \frac{4\,\mathsf{K}(k_z^2)}{z_2}, \tag{49}$$

is the polar period. For example when we have an equation of the form $t(r, z, \lambda) = t_r(r) + t_z(z) + a\mathcal{L}\lambda$ then $\langle t\rangle_z(\lambda) = t_r(r(\lambda)) + \langle t_z\rangle_z(\lambda) + a\mathcal{L}\lambda$. Here the purpose of taking this average is to integrate out the oscillatory dependence and isolate the secular

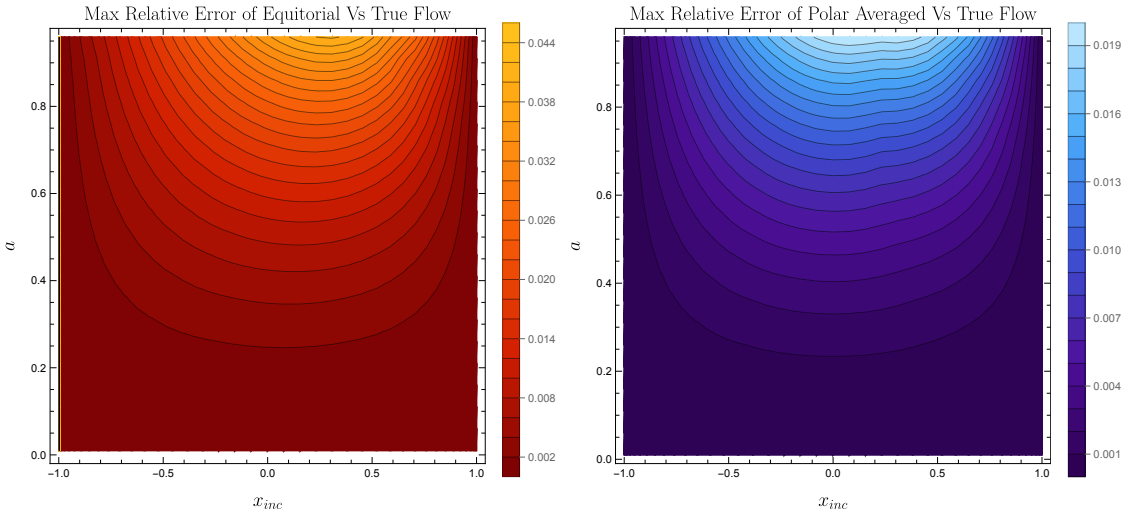

Figure 3. Left Image: Plot of the maximum relative error between the equatorial and true flow over the range (r_+, r_I). Right Image: Plot of the maximum relative error between the polar averaged and true flow over the range (r_+, r_I). Both plots give the error over the entire parameter space (a, x_{inc}).

dependence in λ of terms originally containing polar dependence. Finally, we give the exact equation for the radial inflow as,

$$\frac{dr}{dt} = \frac{-\sqrt{(1-\mathcal{E}^2)(r_I-r)^3(r-\frac{a^2\mathcal{K}}{(1-\mathcal{E}^2)r_I^3})}}{a\mathcal{L}+\frac{(r^2+a^2)}{\Delta}(\mathcal{E}(r^2+a^2)-a\mathcal{L})-a^2\mathcal{E}(1-z_1^2\mathsf{sn}^2\big(\frac{2z_2\sqrt{r-r_4}}{\sqrt{(1-\mathcal{E}^2)(r_I-r)(r_I-r_4)^2}}\big|k_z^2\big))}. \tag{50}$$

Where $\mathsf{sn}(\cdot|\cdot)$ is the Jacobi sine function.

In Fig. 2, which depicts the radial flow from the differing equations, we see an improvement of accuracy in the polar averaged approximation over the equatorial approximation. We also provide a brief error analysis comparing our approximated solutions to the true solution Eq. (50) over the entire parameter space. Here we parameterise our space using (x_{inc}, a) where $x_{inc} = \cos\theta_{inc}$ such that $(x_{inc}, a) \in (\{-1, 1\}, \{0, 1\})$. From Fig. 3 we see that over the parameter space, the equatorial approximation confines the error to be below 5% whilst the polar averaged form provides a bound of 2% maximum relative error. In reality, this is a generous upper bound and for the majority of parameter space the error of the approximated particle inflow will be notably smaller, as can be seen in Fig. 3.

At this stage we are now ready to solve the equations of motion. In the generic case we expect the solutions to arise in terms of elliptic functions. In the ISSO case however, we find that the triple root significantly simplifies the terms with radial dependence to the form of elementary functions. For convenience the solutions for the entirety of the ISSO case are given with initial conditions $(t(\lambda), r(\lambda), z(\lambda), \phi(\lambda))|_{\lambda=0} = (0, r_4, 0, 0)$. The full solution can be easily reconstructed using Eq. (51). Solving Eq. (36) and inverting

the solution gives

$$\lambda(r) = \frac{2\sqrt{r - r_4}}{\sqrt{(1-\mathcal{E}^2)(r_I - r)(r_I - r_4)^2}}, \text{ and} \tag{51}$$

$$r(\lambda) = \frac{r_I(r_I - r_4)^2(1-\mathcal{E}^2)\lambda^2 + 4r_4}{(r_I - r_4)^2(1-\mathcal{E}^2)\lambda^2 + 4}, \tag{52}$$

respectively. The polar solution is unchanged from the generic bound case [39] and given by

$$z(\lambda) = z_1 \sin \xi_z(\lambda). \tag{53}$$

Here we have defined,

$$\xi_z(\lambda) = \mathsf{am}(z_2\lambda | k_z^2), \tag{54}$$

where $\mathsf{am}(\cdot|\cdot)$ is the Jacobi amplitude function. Conveniently for the remaining equations of motion, the polar and radial dependence in the time and azimuthal equation fully decouple from each other in Mino time. This means we are only required to resolve the radial component as the polar part will simply remain the same as has already been found for bound orbits in [38, 39]. The polar dependence still remains in the form of elliptic integrals where $\mathsf{F}(\cdot)$, $\mathsf{E}(\cdot)$ and $\mathsf{\Pi}(\cdot)$ are the elliptic integral of the first, second and third kind respectively. Going on to solve the azimuthal component we first rewrite Eq. (34) as

$$\begin{aligned} d\phi = \frac{-a}{\Delta} \frac{\mathcal{E}(r^2+a^2) - a\mathcal{L}}{\sqrt{(1-\mathcal{E}^2)(r_I - r)^3(r - r_4)}} dr \\ + \frac{\mathcal{L}}{1-z^2} \frac{1}{\sqrt{(z^2 - z_1^2)(a^2(1-\mathcal{E}^2)z^2 - z_2^2)}} dz - a\mathcal{E} d\lambda. \end{aligned} \tag{55}$$

We then integrate each of the terms individually. The component comprising of r dependence is found to be given by,

$$\begin{aligned} \phi_r(\lambda) = a\frac{(\mathcal{E}(r_I^2+a^2) - a\mathcal{L})\lambda}{(r_I - r_-)(r_I - r_+)} + \frac{a}{\sqrt{(1-\mathcal{E}^2)}} \Bigg(\frac{(\mathcal{E}(r_-^2+a^2) - a\mathcal{L})}{2\sqrt{r_- - r_4}(r_I - r_-)^{\frac{3}{2}}(r_+ - r_-)} \times \\ \log\left(\frac{\left(2\sqrt{r_- - r_4} + \lambda(r_I - r_4)\sqrt{(1-\mathcal{E}^2)(r_I - r_-)}\right)^2}{\left(2\sqrt{r_- - r_4} - \lambda(r_I - r_4)\sqrt{(1-\mathcal{E}^2)(r_I - r_-)}\right)^2} \right) + (r_- \longleftrightarrow r_+) \Bigg), \end{aligned} \tag{56}$$

where the arrow notation denotes taking the other term within the shared brackets and swapping all occurrences of r_- with r_+. The component with z dependence is then given by,

$$\phi_z(\lambda) = \frac{\mathcal{L}}{z_2} \mathsf{\Pi}(z_1^2; \xi_z(\lambda) | k_z^2). \tag{57}$$

The polar average form of this solution can also be found and dramatically simplifies the functional dependence,

$$\langle \phi_z \rangle_z(\lambda) = \frac{\mathcal{L}}{\mathsf{K}(k_z^2)} \mathsf{\Pi}(z_1^2; k_z^2)\lambda, \tag{58}$$

where $\Pi(\cdot,\cdot)$ is the complete elliptic integral of the third kind. Thus, we find the full azimuthal solution to be given by

$$\phi(\lambda) = \phi_r(\lambda) + \phi_z(\lambda) - a\mathcal{E}\lambda. \tag{59}$$

We perform a similar separation in the integration of the equation of motion for coordinate time giving,

$$\begin{aligned} t_r(\lambda) = &\frac{(a^2+r_I^2)(\mathcal{E}(r_I^2+a^2)-a\mathcal{L})\lambda}{(r_I-r_-)(r_I-r_+)} + \frac{2(r_I-r_4)^2\mathcal{E}\lambda}{4+(1-\mathcal{E}^2)(r_I-r_4)^2\lambda^2} \\ &- \frac{(r_4+3r_I+2(r_++r_-))}{\sqrt{(1-\mathcal{E}^2)}}\mathcal{E}\arctan\left(\frac{\lambda(r_I-r_4)\sqrt{(1-\mathcal{E}^2)}}{2}\right) \\ &+ \left(\frac{(a^2+r_-^2)(\mathcal{E}(r_-^2+a^2)-a\mathcal{L})}{2\sqrt{r_--r_4}(r_I-r_-)^{\frac{3}{2}}(r_+-r_-)\sqrt{(1-\mathcal{E}^2)}}\times\right. \\ &\left.\log\left(\frac{\left(2\sqrt{r_--r_4}+\lambda(r_I-r_4)\sqrt{(1-\mathcal{E}^2)(r_I-r_-)}\right)^2}{\left(2\sqrt{r_--r_4}-\lambda(r_I-r_4)\sqrt{(1-\mathcal{E}^2)(r_I-r_-)}\right)^2}\right) + (r_- \Longleftrightarrow r_+)\right). \end{aligned} \tag{60}$$

Next we find the polar dependent part of the time solution to be given by,

$$t_z(\lambda) = \frac{\mathcal{E}}{1-\mathcal{E}^2}\left((z_2^2 - a^2(1-\mathcal{E}^2))\lambda - z_2\,\mathsf{E}(\xi_z(\lambda)|k_z^2)\right), \tag{61}$$

and the polar averaged form of this solution is given by,

$$\langle t_z\rangle_z(\lambda) = \frac{z_2^2\mathcal{E}}{1-\mathcal{E}^2}\left(1 - \frac{a^2(1-\mathcal{E}^2)}{z_2^2} - \frac{\mathsf{E}(k_z^2)}{\mathsf{K}(k_z^2)}\right)\lambda. \tag{62}$$

This is the expression that was necessary to derive the polar averaged radial flow in Eq. (47). Putting this all together we then find the time solution to be given by

$$t(\lambda) = t_r(\lambda) + t_z(\lambda) + a\mathcal{L}\lambda. \tag{63}$$

We find that all of the novel radial integrals which are required to be solved can be done so without too much issue through the use of partial fractions. They can then be fully analytically continued by applying some simple trigonometric substitutions.

Additionally one can follow this approach to find the solution for proper time as a function of Mino time along a plunging ISSO geodesic,

$$\begin{aligned} \tau_r(\lambda) = &\left(r_I^2 + \frac{2(r_I-r_4)^2}{4+(1-\mathcal{E}^2)(r_I-r_4)^2\lambda^2}\right)\lambda \\ &+ \frac{(r_4^2+2r_4r_I-3r_I^2)\arctan(\frac{\lambda(r_I-r_4)\sqrt{(1-\mathcal{E}^2)}}{2})}{\sqrt{(1-\mathcal{E}^2)}(r_I-r_4)}, \end{aligned} \tag{64}$$

$$\tau_z(\lambda) = \frac{z_2}{(1-\mathcal{E}^2)}\left(F(\xi_z\,|k_z^2) - E(\xi_z\,|k_z^2)\right), \text{ with} \tag{65}$$

$$\tau(\lambda) = \tau_r(\lambda) + \tau_z(\lambda). \tag{66}$$

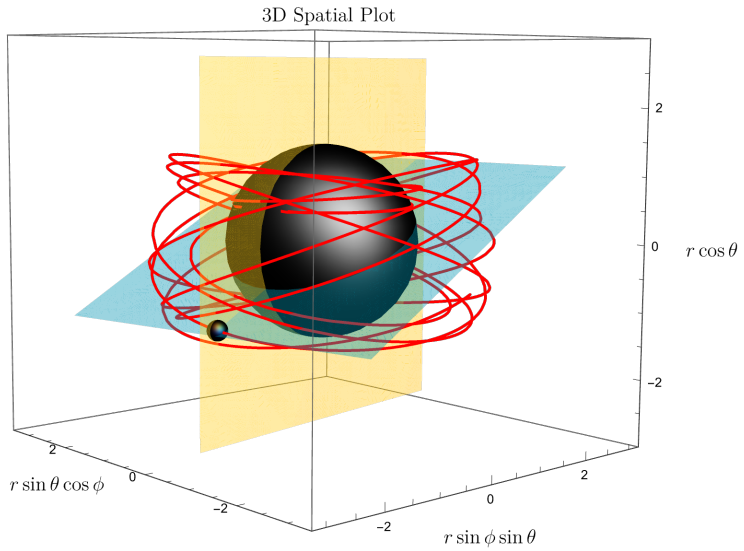

Figure 4. Orbital plots of plunging geodesics which asymptote to the ISSO in the infinite past with $(a, r_I) = (0.9, 2.6)$ and $\theta = \arccos(z)$. Here the cyan and orange planes are the azimuthally co-precessing and poloidally co-rotating planes respectively. Examples of the projection on these planes are shown in Fig. 5.

From Fig. 4 it can now be seen explicitly that enforcing the triple root places us in a regime where these geodesics asymptote from the ISSO and subsequently plunge in through the horizon. This showcases a number of properties of the plunge in Boyer-Lindquist co-ordinates. The structure of these geodesics is more easily depicted when orthogonally projected onto azimuthally co-precessing and poloidally co-rotating planes fixed to a particle as it follows the geodesic. In Fig. 5 we see that the azimuthal coordinate diverges at both the inner and outer horizons. Analysis of the coordinate time solution shows it also diverges at these points, this occurs for a similar reason as to the coordinate time divergence at the horizon in Schwarzschild coordinates for a non-spinning black hole, i.e. due to the infinite redshift. In much the same way as we have an infinite redshift on the horizon one can intuitively think of this azimuthal divergence occurring as a consequence of the infinite redshift on the horizon forcing the geodesics to also co-rotate with the black hole an infinite number of times before passing through the horizon. Naturally this is only a co-ordinate singularity and the process occurs in finite Mino and proper time. Due to this discontinuity care must be taken in the choice of branch between r_+ and r_-. The solutions depicted in 4 and 5 seem to invert between the horizons but it can be checked that our solutions conserve $\mathcal{E}, \mathcal{L}$ and $\mathcal{K}$ throughout their parameterisation, confirming we have chosen the correct branch. In the equatorial ($\mathcal{K} = 0$) limit, these solutions are found to agree with the results of [42].

In the interest of completeness, we also derived the solutions for plunging geodesics asymptoting from a generic USO. In the phase space of geodesics, the USOs denote the separatrix between eccentric inclined bound orbits and generic plunges. As such, they play a key role when considering the transition of generic inspirals to plunge. As

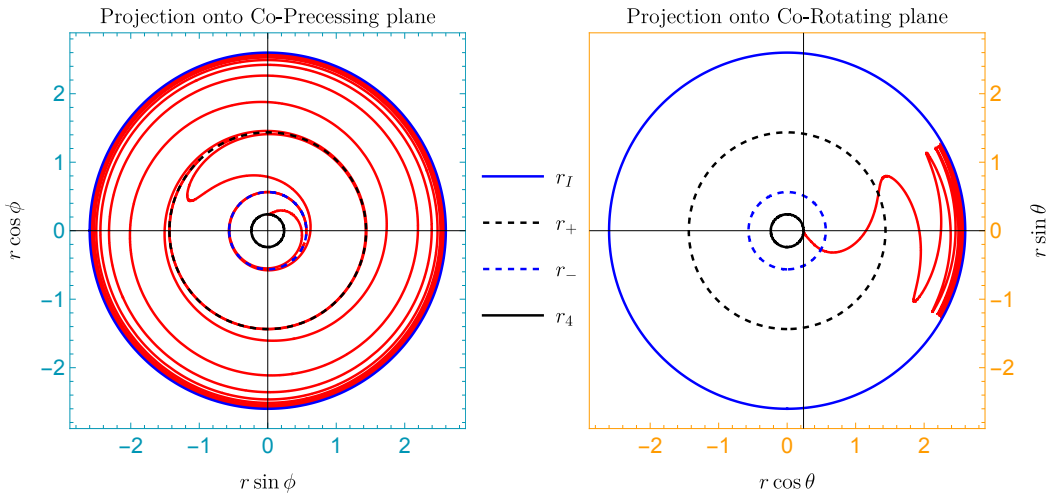

Figure 5. Co-rotating orbital plots of plunging geodesics which asymptote to the ISSO in the infinite past with $(a, r_I) = (0.9, 2.6)$. Left Image: orthogonal projection of ISSO plunge onto the co-precessing azimuthal plane. Right Image: orthogonal projection of ISSO plunge onto co-rotating polar plane. The cyan and orange frames represent the projection onto the planes seen in 4 as they track a particle following the geodesic trajectory.

mentioned previously the components of the solutions depending on the polar angle are left unchanged by restricting to this special case so we are only required to solve for $r(\lambda)$, $\phi_r(\lambda)$ and $t_r(\lambda)$. In particular, plunges from an USO occur when the radial potential obtains a double root as opposed to a triple root (which arises in the ISSO case). Explicitly the USO plunge occurs when the radial potential admits a form,

$$R(r) = (1 - \mathcal{E}^2)(r - r_2)(r_1 - r)(r_s - r)^2 \,, \tag{67}$$

with $r_2 < r_- < r_+ < r_s < r_1$. Where r_s is the radius of the USO. Specifically, the solutions we present provide bound motion for $r \in (r_2, r_s)$. The Penrose diagram depicting this class of motion is the same as in Fig. 1 for the ISSO plunges. As we have imbued the radial potential with a double root we have reduced one degree of freedom in our systems parameterisation. A natural choice of parameterisation for USO plunges is then given by $\{a, r_s, \mathcal{K}\}$. Teo [71] has determined expressions for $\mathcal{E}$ and $\mathcal{L}$ as functions of $\{a, r_s, \mathcal{K}\}$ for the case of USOs which are given as,

$$\mathcal{E} = \frac{r_s^3(r_s - 2) - a(a\,\mathcal{K} - \sqrt{A})}{r_s^2\sqrt{r_s^3(r_s - 3) - 2a(a\,\mathcal{K} - \sqrt{A})}} \,, \tag{68}$$

$$\mathcal{L} = -\frac{2Mr_s^3 + (r_s^2 + a^2)(a\,\mathcal{K} - \sqrt{A})}{r_s^2\sqrt{r_s^3(r_s - 3) - 2a(a\,\mathcal{K} - \sqrt{A})}} \,, \tag{69}$$

where

$$A = r_s^5 - \mathcal{K}(r_s - 3)r_s^3 + a^2\,\mathcal{K}^2 \,. \tag{70}$$

As USO plunges asymptote from the USO they must share the same constants of motion. Similarly to the case of the ISSO the reduced complexity in the root structure of the radial potential allows one to find solutions to the radial integrals fully in terms of elementary functions of Mino time. Following the procedure shown explicitly in section 4 and defining,

$$\xi_r(\lambda) = \frac{1}{2}\lambda\sqrt{1-\mathcal{E}^2}\sqrt{r_1-r_s}\sqrt{r_s-r_2}\,, \tag{71}$$

the solution for the radial coordinate is found to be given by,

$$r(\lambda) = \frac{r_2\left(r_1-r_s\right)+r_1\left(r_s-r_2\right)\tanh^2\left(\xi_r\right)}{r_1-r_s+\left(r_s-r_2\right)\tanh^2\left(\xi_r\right)}. \tag{72}$$

Writing the azimuthal equation in the form $\phi(\lambda) = \phi_r(\lambda) + \phi_z(\lambda) - a\mathcal{E}\lambda$ and the time equation in the form $t(\lambda) = t_r(\lambda) + t_z(\lambda) + a\mathcal{L}\lambda$ we find that for the case of timelike geodesics asymptoting from an USO,

$$\begin{aligned}\phi_r(\lambda) = \frac{2a}{\sqrt{1-\mathcal{E}^2}}\Bigg(&\frac{\lambda\sqrt{1-\mathcal{E}^2}\left(a^2\mathcal{E}-a\mathcal{L}+\mathcal{E}r_s^2\right)}{2\left(r_s-r_-\right)\left(r_s-r_+\right)} \\ &+\frac{\left(a^2\mathcal{E}-a\mathcal{L}+r_-^2\mathcal{E}\right)\log\left(\frac{\left(\sqrt{(r_--r_2)(r_1-r_s)}+\sqrt{(r_1-r_-)(r_s-r_2)}\tanh(\xi_r)\right)^2}{\left(\sqrt{(r_--r_2)(r_1-r_s)}-\sqrt{(r_1-r_-)(r_s-r_2)}\tanh(\xi_r)\right)^2}\right)}{4\left(r_--r_+\right)\sqrt{r_1-r_-}\sqrt{r_--r_2}\left(r_--r_s\right)} \\ &+\frac{\left(a^2\mathcal{E}-a\mathcal{L}+r_+^2\mathcal{E}\right)\log\left(\frac{\left(\sqrt{(r_--r_2)(r_1-r_s)}+\sqrt{(r_1-r_+)(r_s-r_2)}\tanh(\xi_r)\right)^2}{\left(\sqrt{(r_+-r_2)(r_1-r_s)}-\sqrt{(r_1-r_+)(r_s-r_2)}\tanh(\xi_r)\right)^2}\right)}{4\left(r_+-r_-\right)\sqrt{r_1-r_+}\sqrt{r_+-r_2}\left(r_+-r_s\right)}\Bigg),\end{aligned} \tag{73}$$

and,

$$\begin{aligned}t_r(\lambda) = \frac{1}{\sqrt{1-\mathcal{E}^2}}\Bigg(&\frac{\lambda\sqrt{1-\mathcal{E}^2}\left(a^2+r_s^2\right)\left(a^2\mathcal{E}-a\mathcal{L}+\mathcal{E}r_s^2\right)}{\left(r_s-r_-\right)\left(r_s-r_+\right)} \\ &+\frac{\left(a^2+r_-^2\right)\left(a^2\mathcal{E}-a\mathcal{L}+r_-^2\mathcal{E}\right)\log\left(\frac{\left(\sqrt{r_--r_2}\sqrt{r_1-r_s}+\sqrt{r_1-r_-}\sqrt{r_s-r_2}\tanh(\xi_r)\right)^2}{\left(\sqrt{r_--r_2}\sqrt{r_1-r_s}-\sqrt{r_1-r_-}\sqrt{r_s-r_2}\tanh(\xi_r)\right)^2}\right)}{2\left(r_--r_+\right)\sqrt{r_1-r_-}\sqrt{r_--r_2}\left(r_--r_s\right)} \\ &+\frac{\left(a^2+r_+^2\right)\left(a^2\mathcal{E}-a\mathcal{L}+r_+^2\mathcal{E}\right)\log\left(\frac{\left(\sqrt{r_+-r_2}\sqrt{r_1-r_s}+\sqrt{r_1-r_+}\sqrt{r_s-r_2}\tanh(\xi_r)\right)^2}{\left(\sqrt{r_+-r_2}\sqrt{r_1-r_s}-\sqrt{r_1-r_+}\sqrt{r_s-r_2}\tanh(\xi_r)\right)^2}\right)}{2\left(r_+-r_-\right)\sqrt{r_1-r_+}\sqrt{r_+-r_2}\left(r_+-r_s\right)} \\ &+\frac{\left(r_1-r_2\right)\mathcal{E}\sqrt{\left(r_1-r_s\right)\left(r_s-r_2\right)}\tanh\left(\xi_r\right)}{-\left(\left(r_2-r_s\right)\tanh^2\left(\xi_r\right)\right)-r_s+r_1} \\ &-\mathcal{E}\left(2\left(r_s+r_-+r_+\right)+r_1+r_2\right)\tan^{-1}\left(\frac{\sqrt{r_s-r_2}\tanh\left(\xi_r\right)}{\sqrt{r_1-r_s}}\right)\Bigg).\end{aligned} \tag{74}$$

Where ϕ_z and t_z are left unchanged from Eqs. 57 and 61. In the equatorial limit ($\mathcal{K} = 0$) these solutions agree with the equatorial plunging orbits described in section V.C of [74],

where the radius of the unstable circular orbit is chosen between the innermost bound circular orbit (IBCO) and the ISCO.

5. Fully Generic Plunging Orbits in Kerr

We now move on to the case of generic timelike plunging geodesics in Kerr with no restriction on the root structure of the effective radial potential. In this regime the integrals we need to compute are notably more involved, separating into two primary classes. The first being when the radial potential admits four real roots and the second being when the radial potential admits two real and two complex roots. In the case with $R(r)$ having four real roots ($r_4 < r_3 < r_2 < r_1$) with $r_4 < r_- < r_+ < r_3 < r_2 < r_1$ the solution can be directly borrowed from the bound orbit case [38, 39] with the substitution $r_1 \Longleftrightarrow r_3$ and $r_2 \Longleftrightarrow r_4$. In addition, in the case of 4 real roots ($r_4 < r_3 < r_2 < r_1$) with $r_4 < r_3 < r_2 < r_- < r_+ < r_1$ then the solutions can again be found from [38, 39], this time with no modification. Naively, in the case of two real and two complex roots (the interesting case for self-force plunges) one may think it to be sufficient to simply take the previously found bound solutions and analytically continue them to allow for complex values of the radial roots. With care this can be done to give correct answers, however intermediate terms in the evaluations give rise to large cancellations between complex numbers affecting numerical accuracy and evaluation speed. To find these solutions in a manifestly real, easy-to-evaluate, and practical manner, we are required to begin the procedure of solving the complicated elliptic integrals from scratch.

In calculating the integrals for this case we follow the procedure outlined in [75] and give an overview of the steps involved. We begin by again noting that only the radial components of each of the equations need to be solved as the other remaining terms are identical to those already found in the ISSO case above. Recall we now have the general expression $R(r) = (\mathcal{E}(r^2+a^2) - a\mathcal{L})^2 - \Delta(r^2 + (a\mathcal{E} - \mathcal{L})^2 + \mathcal{K})$ where $\mathcal{E}$, $\mathcal{L}$ and $\mathcal{K}$ are all independent quantities. At this stage the integrals of concern are given by

$$\begin{aligned} \lambda &= -\int \frac{dr'}{\sqrt{R(r')}}, \\ t_r(r) &= -\int \frac{(r'^2+a^2)(\mathcal{E}(r'^2+a^2) - a\mathcal{L})dr'}{\Delta\sqrt{R(r')}}, \quad \text{and} \\ \phi_r(r) &= -\int \frac{a(\mathcal{E}(r'^2+a^2) - a\mathcal{L})dr'}{\Delta\sqrt{R(r')}}. \end{aligned} \tag{75}$$

Although these integrals look to be of the same form as those we just solved for in the ISSO case without much mention, the cause for the substantial increase in complexity is due to the fact that $R(r)$, in general, no longer contains any double or triple roots. This forces us to much more carefully consider the elliptic integrals at hand. The key idea in the procedure we wish to apply is to reduce the integrals of Eq. 75 such that we

must only solve integrals of the form,

$$\begin{aligned}\lambda &= -\int \frac{dr}{\sqrt{R(r)}}, \quad \mathcal{I}_r = \int \frac{rdr}{\sqrt{R(r)}}, \\ \mathcal{I}_{r^2} &= \int \frac{r^2 dr}{\sqrt{R(r)}}, \text{ and } \mathcal{I}_{r_\pm} = \int \frac{dr}{(r-r_\pm)\sqrt{R(r)}}.\end{aligned} \tag{76}$$

We solve these integrals in terms of the radial co-ordinate r, which can then be parameterised in terms of Mino time by inverting the solution for $\lambda(r)$. We begin solving these integrals by first continually applying partial fractions to the radial parts of the ϕ and t equations until arriving at the forms,

$$\phi_r = a\left(\frac{(\mathcal{E}(r_-^2+a^2)-a\mathcal{L})}{(r_- - r_+)}\mathcal{I}_{r_-} + (r_- \longleftrightarrow r_+)\right) + a\mathcal{E}\lambda, \text{ and} \tag{77}$$

$$\begin{aligned}t_r = {} & \mathcal{E}(r_+^2 + r_-^2 + r_+r_- + 2a^2)\lambda + \mathcal{E}\left(\mathcal{I}_{r^2} + \mathcal{I}_r(r_- + r_+)\right) \\ & + \left(\frac{(r_-^2+a^2)(\mathcal{E}(r_-^2+a^2)-a\mathcal{L})}{r_- - r_+}\mathcal{I}_{r_-} + (r_- \longleftrightarrow r_+)\right) - a\mathcal{L}\lambda.\end{aligned} \tag{78}$$

At this point we can now concentrate on calculating the four elliptic integrals defined in Eq.(76). We do this my applying a transformation given for the case of two complex roots in [75]. This procedure begins by letting $R(r)$ have two real roots $r_2 < r_1$ and two complex roots r_3 and r_4. We then rewrite $R(r)$ in the form $R(r) = (1-\mathcal{E}^2)(r_1 - r)(r - r_2)(r^2 - 2\rho_r r + \rho_r^2 - \rho_i^2)$ where $\rho_r = \Re(r_3)$ and $\rho_i = \Im(r_4)$. Further we define

$$\begin{aligned}A &= \sqrt{(r_1-\rho_r)^2 + \rho_i^2}, \quad B = \sqrt{(r_2-\rho_r)^2 + \rho_i^2}, \\ f &= \frac{4AB}{(A-B)^2}, \quad k_r = \sqrt{\frac{(r_1-r_2)^2 - (A-B)^2}{4AB}}, \text{ and} \\ p_2 &= r_2A^2 + r_1B^2 - (r_1+r_2)AB.\end{aligned} \tag{79}$$

Next, motivated by the tables provided in [75], we make the substitution in the integrals Eq. (76) of the form,

$$r(y) = \frac{p_2y^2 + 2(r_1+r_2)AB + 2(r_1-r_2)AB\sqrt{1-y^2}}{(A-B)^2y^2 + 4AB}. \tag{80}$$

Applying this transformation to Eq. (76) and again repeatedly applying partial fractions we find each integral reduces to a sum over elliptic integrands and rational polynomials. The solutions we then obtain are only analytic on the range $r \in (r_2, \frac{r_1A+r_2B}{A+B})$ where for convenience we have set the initial conditions to be given by $(t(\lambda), r(\lambda), z(\lambda), \phi(\lambda))|_{\lambda=0} = (0, r_2, 0, 0,)$. Next we analytically extend these solutions through the point $r = \frac{r_1A+r_2B}{A+B}$ by use of trigonometric and elliptic substitutions providing a fully analytic solution on the range $r \in (r_2, r_1)$. The fully analytical solution to these integrals is then given by

$$\int \frac{dr}{\sqrt{R(r)}} = \frac{1}{\sqrt{(1-\mathcal{E}^2)AB}}\mathsf{F}\left(\frac{\pi}{2} - \arcsin\left(\frac{B(r_1-r) - A(r-r_2)}{B(r_1-r) + A(r-r_2)}\right)\middle| k_r^2\right), \tag{81}$$

$$\mathcal{I}_r(\lambda) = \frac{Ar_2 - Br_1}{A-B}\lambda - \frac{1}{\sqrt{(1-\mathcal{E}^2)}}\arctan\left(\frac{(r_1-r_2)}{2\sqrt{AB}}\frac{\sin(\xi_{\rm r})}{\sqrt{1-k_r^2\sin(\xi_{\rm r})^2}}\right) + \frac{(A+B)(r_1-r_2)}{2(A-B)\sqrt{(1-\mathcal{E}^2)AB}}\,\Pi\left(-\frac{1}{f};\xi_{\rm r}\,|k_r^2\right), \tag{82}$$

$$\begin{aligned}\mathcal{I}_{r^2}(\lambda) = {} & \frac{(Ar_2^2 - Br_1^2)}{(A-B)}\lambda + \frac{\sqrt{AB}}{(1-\mathcal{E}^2)}\,\mathsf{E}\left(\xi_{\rm r}\,|k_r^2\right) \\ & - \frac{(A+B)(A^2+2r_2^2-B^2-2r_1^2)}{4(A-B)\sqrt{(1-\mathcal{E}^2)AB}}\,\Pi(-\frac{1}{f};\xi_{\rm r}\,|k_r^2) \\ & - \frac{\sqrt{AB}(A+B-(A-B)\cos(\xi_{\rm r}))}{(A-B)\sqrt{(1-\mathcal{E}^2)}}\frac{\sin(\xi_{\rm r})\sqrt{1-k_r^2\sin(\xi_{\rm r})^2}}{(f+\sin(\xi_{\rm r})^2)} \\ & + \frac{A^2+2r_2^2-B^2-2r_1^2}{4(r_1-r_2)\sqrt{(1-\mathcal{E}^2)}}\times \\ & \arctan\left(f-(1+2fk_r^2)\sin^2(\xi_r), 2\sin(\xi_r)\sqrt{1-k_r^2\sin^2(\xi_r)}\sqrt{f(1+fk_r^2)}\right),\end{aligned} \tag{83}$$

and,

$$\begin{aligned}\mathcal{I}_{r_\pm}(\lambda) = {} & \frac{(A-B)\lambda}{A(r_2-r_\pm)-B(r_1-r_\pm)} \\ & + \frac{(r_1-r_2)(A(r_2-r_\pm)+B(r_1-r_\pm))\,\Pi\left(\frac{1}{D_\pm^2};\xi_{\rm r}\,|k_r^2\right)}{2\sqrt{(1-\mathcal{E}^2)AB}(r_\pm-r_2)(r_1-r_\pm)(A(r_2-r_\pm)-B(r_1-r_\pm))} \\ & - \frac{\sqrt{r_1-r_2}}{4\sqrt{(1-\mathcal{E}^2)(r_1-r_\pm)(r_\pm-r_2)}}\times \\ & \frac{\log\left(\frac{\left(D_\pm\sqrt{1-D_\pm^2k_r^2}+\sqrt{1-k_r^2\sin(\xi_{\rm r})^2}\sin(\xi_{\rm r})\right)^2+\left(k_r(D_\pm^2-\sin(\xi_{\rm r})^2)\right)^2}{\left(D_\pm\sqrt{1-D_\pm^2k_r^2}-\sqrt{1-k_r^2\sin(\xi_{\rm r})^2}\sin(\xi_{\rm r})\right)^2+\left(k_r(D_\pm^2-\sin(\xi_{\rm r})^2)\right)^2}\right)}{\sqrt{(A^2(r_\pm-r_2)-(r_1-r_\pm)(r_2^2-B^2+r_1r_\pm-r_2(r_1+r_\pm))}}.\end{aligned} \tag{84}$$

Where we have defined,

$$D_\pm = \frac{\sqrt{4AB(r_1-r_\pm)(r_\pm-r_2)}}{A(r_\pm-r_2)+B(r_\pm-r_1)}\ , \text{and} \tag{85}$$

$$\xi_r(\lambda) = \mathsf{am}(\sqrt{(1-\mathcal{E}^2)AB}\lambda|k_r^2). \tag{86}$$

In the above we have suppressed the explicit dependence of ξ_r on λ in the interest of readability. The arctan function seen in Eq. (83) is the two argument arctan function which tracks the sectors of the numerator and denominator.

The solution for Eqs. (81)-(84) for the elliptic integrals can then be readily substituted back into Eq. (77) and Eq. (78) giving the full form of the solutions to

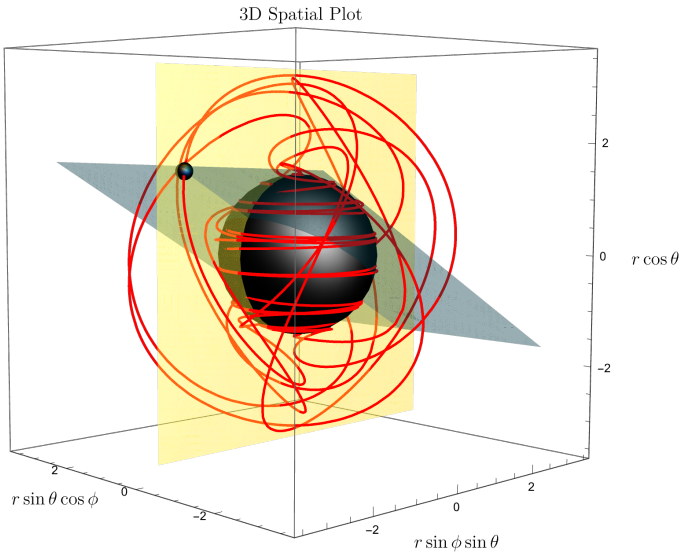

Figure 6. Orbital plot of a generic plunging geodesic with parameter values $(a, \mathcal{E}, \mathcal{L}, \mathcal{K}) = (0.9, 0.94, 0.1, 12)$ and $\theta = \arccos(z)$. The larger black sphere gives the horizon of the black hole where as the smaller sphere simply gives a point along the geodesics. Here the cyan and orange planes are the azimuthally co-precessing and poloidally co-rotating planes respectively.

generic plunges. We present all solutions parameterised in terms on Mino time (λ), which is done by inverting the solution to Eq. (81) to obtain $r(\lambda)$ then substituting the solution for $r(\lambda)$ everywhere r appears in Eqs. (82)-(84) . These solutions are provided in a fully analytic form. The radial equation is first found by inverting the solution for Eq. (81) to give,

$$r(\lambda) = \frac{(A-B)(Ar_2 - Br_1)\sin(\xi_{\rm r})^2 + 2AB(r_2+r_1) - 2AB(r_1-r_2)\cos(\xi_{\rm r})}{4AB + (A-B)^2\sin(\xi_{\rm r})^2}. \tag{87}$$

The solutions to the polar equation remain the same as for the ISSO case. Taking Eq. (77), the solution to the azimuthal equations of motion can then immediately be found from the solutions of Eq. (76)

$$\phi(\lambda) = \phi_r(\lambda) + \phi_z(\lambda) - a\mathcal{E}\lambda. \tag{88}$$

Similarly, from Eq. (78) we can now obtain

$$t(\lambda) = t_r(\lambda) + t_z(\lambda) + a\mathcal{L}\lambda, \tag{89}$$

where both ϕ_z and t_z can be taken from the ISSO case. The solution for proper time as a function of Mino time can also be found as,

$$\tau(\lambda) = \tau_r(\lambda) + \tau_z(\lambda), \text{ with} \tag{90}$$

$$\tau_r(\lambda) = \mathcal{I}_{r^2}(\lambda), \text{ and} \tag{91}$$

$$\tau_z(\lambda) = \frac{z_2}{(1-\mathcal{E}^2)}\left(F(\xi_{\rm z}\,|k_z^2) - E(\xi_{\rm z}\,|k_z^2)\right). \tag{92}$$

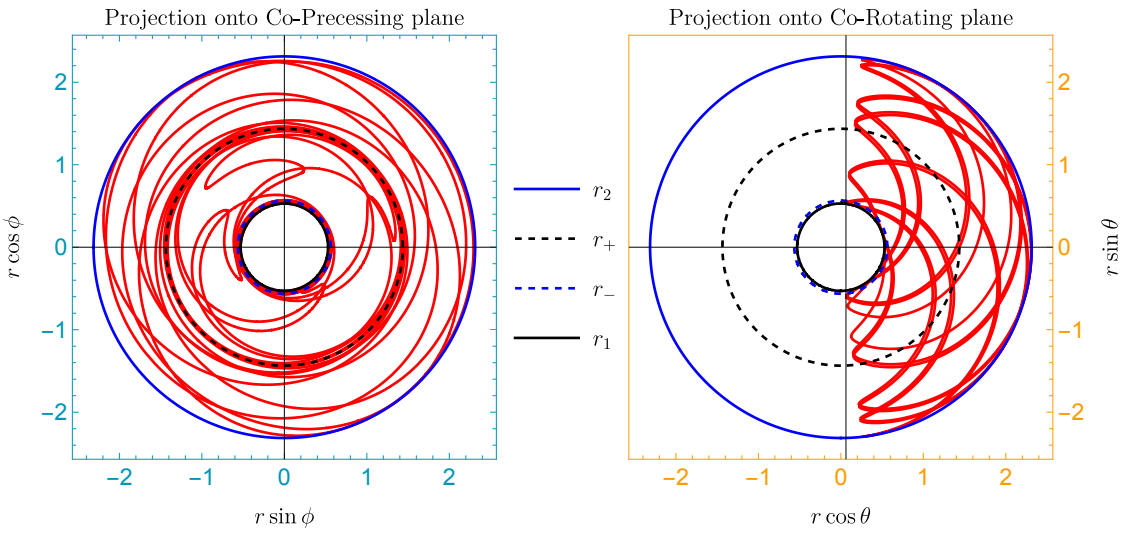

Figure 7. Co-rotating orbital plots of a generic plunging geodesic with parameter values $(a, \mathcal{E}, \mathcal{L}, \mathcal{K}) = (0.9, 0.94, 0.1, 12)$. Left Image: orthogonal projection of generic plunge onto the co-precessing azimuthal plane. Right Image: orthogonal projection of generic plunge onto co-rotating polar plane. The cyan and orange frames represent the projection onto the planes seen in 6 as they track a particle following the geodesic trajectory.

Having obtained the full set of solutions for generic plunges we plot the spatial component depicting the orbital evolution of the generic plunging geodesics Fig. 6. More informatively, the orthogonal projection onto the azimuthally co-precessing and poloidally co-rotating planes in Fig. 7 again show the divergences at either horizon in the ϕ coordinate. Importantly, once we have constructed these solution, we check that $\mathcal{E}$ and $\mathcal{L}$ are indeed still conserved by evaluating $-u^\nu g_{\mu\nu}\left(\frac{\partial}{\partial t}\right)^\nu$ and $u^\nu g_{\mu\nu}\left(\frac{\partial}{\partial \phi}\right)^\nu$ explicitly. We confirm this is the case for all values of λ, not only acting as a consistency check of our equations, but also showing we have selected the correct branches of the solution between each of the horizon divergences. As a final consistency check, we substitute our solutions back into the equations of motion for both the ISSO and generic case and find that our solutions do in fact solve the original equations. Finally, from our solutions the radial and polar frequencies with respect to Mino time for a generic plunge can be found to be,

$$\Upsilon_r = \frac{\sqrt{AB(1-\mathcal{E}^2)}}{2\,\mathsf{K}(k_r^2)}, \text{ and} \tag{93}$$

$$\Upsilon_z = \frac{\pi\,\mathsf{K}(k_z^2)}{2z_2}. \tag{94}$$

6. The Particle Motion and Cosmic Censorship in Dyonic KN

The fundamentally novel motion which can occur in dyonic KN spacetimes as opposed to the neutral Kerr configuration is one that has seen little exploration in the past. Here

we attempt to shed light on the dynamics of these systems. Doing so we now reinstate the parameters $\{e, g, P, Q\}$ as being nonzero quantities. Using similar methods to those outlined in section 5 we solve the dyonic equations of motion in KN analytically for generic plunging and bound geodesics in terms of Jacobi Elliptic functions. In carrying out this work we also developed a `Mathematica` package implementing these solutions which is now publically available on `Github`. The code is built using the same structure as the KerrGeodesics package of the Black Hole Perturbation Toolkit [3].

The purpose of this section however is not to outline how the equations of motion were solved, as the process follows very closely to that of section 5. Instead, the focus here will be to outline some of the key differences between dyonic motion in KN and particle motion in Kerr. Firstly we note in the dyonic case both the energy and angular momentum defined in 22 and 23 receive non-trivial contributions from the electromagnetic momentum maps. Notably, if $\Omega \neq 0$ the angular momentum of the system is nonzero, even if the particle exhibits purely radial motion along the axis $(\theta = 0, \pi)$. Another difference also presents itself in the interpretation of $\mathcal{K}$. In the case of neutral particles, one finds that bound $(\mathcal{E}^2 < 1)$ geodesics with $\mathcal{K} = 0$ are necessarily confined to the equator $(z = 0)$. This is clearly no longer the case if $\Omega \neq 0$, even if the black hole is non-rotating $a = 0$. Thus, unless the configuration is purely electric or neutral, $\mathcal{K}$ can no more be interpreted as a measure of off-equatorial motion. We also find that in KN if charged or neutral particles wish to hit the curvature singularity (the ring $r^2 + a^2 z^2 = 0$) they must have $\mathcal{K} = 0$ and $\mathcal{L} = a\mathcal{E}$, as follows immediately by requiring that $R(0) \geq 0$ and $Z(0) \geq 0$, the second of these constraints does not arise in Kerr.

In the analysis of the gravitational and electromagnetic fields one finds that the key factor which leads to qualitatively new dynamics is the existence of a dipolar electric field which is induced by the spinning magnetic charge. This leads to an equatorial asymmetry in the sign of the field strength tensor,

$$F_{\mu\nu}\left(r, \pi - \theta\right) = -F_{\mu\nu}\left(r, \theta\right) \ . \tag{95}$$

An immediate consequence of this asymmetry is that, unlike in rotating magnetised

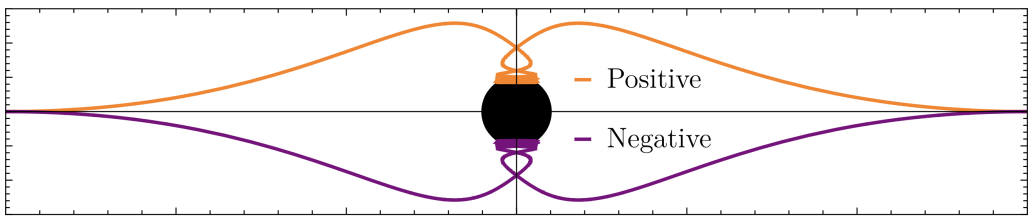

Figure 8. This figure shows the evolution of two pairs of electric particles on a magnetic KN black hole. Each pair has two particles with identical initial conditions at the equator, but opposite charge signs. As discussed in the text, the motion of positive and negative charges are the mirror image of each other with respect to the equator.

electric black holes, rotating magnetic ones will not tend to grow a net Wald charge when immersed on an ionised homogeneous medium. This fact can be understood as a consequence that every point on the horizon which accretes some charge q will have a corresponding point under reflection in the equatorial plane which accretes precisely the opposite amount of charge $-q$ which can be seen in Fig. 8 . This conclusion also follows by inspection of the black hole's electric potential, ϕ, which is given by,

$$\phi = -\mathcal{P}_k|_{\mathcal{H}^+}, \tag{96}$$

where k is the Killing vector that generates $\mathcal{H}^+$, and $\mathcal{P}_k$ is the associated electric momentum map given by Eq. (17). If the black hole has no electric charge, as in our case, then ϕ vanishes indicating that accretion of a net electric charge is not energetically favored, thus a hole imbued with magnetic charge will remain globally neutral with respect to electric charges even when immersed in an ionised homogeneous medium.

Restricting our attention solely along the axis one can also glean some profoundly novel consequences of the dyonic KN structure. Namely, for an electrically charged particle, confined to exhibit radial motion along the axis of a magnetically charged KN black hole the angular momentum of the particle, given by Eq. 23, is found to be,

$$\mathcal{L} = \begin{cases} -Pe/m & (\ \theta = 0) \\ +Pe/m & (\ \theta = \pi) \end{cases}. \tag{97}$$

This result, which at first may seem to be quite striking, has however a basis in the physics of the early 20th century. In fact, if one considers the non-gravitating case of a static electric and magnetic charge held at a fixed radius from one another, one also arrives at a system with non-vanishing angular momentum. These systems were first studied by Thompson in 1904 (henceforth referred to as Thompson dipoles) [76] who pointed out that, in spite of being axially symmetric and static, the electromagnetic field in these setups possesses a non-vanishing angular momentum which is independent of the distance between charges. It is given by

$$\vec{J} = \frac{1}{4\pi}\int_{R^3} \vec{r} \wedge \left(\vec{E} \wedge \vec{B}\right) dx^3 = -eg\ \hat{r}\,, \tag{98}$$

where $\hat{r}$ is the unit vector pointing from the magnetic charge into the electric one. This surprising fact provides a way of obtaining Dirac's quantisation condition by assuming that $|\vec{J}|$ is quantised in half-integer units of $\hbar$ [77, 78], so

$$2ge/\hbar = 0, \pm 1, \pm 2, ... \in Z\,. \tag{99}$$

One way of generalising this picture to include gravitation consists in replacing the magnetic point charge g by a magnetic black hole with charge P. This was first considered in [79] and independently later in [80], where the authors considered the process of dropping an electric charge radially into a non-rotating magnetic black hole (see also [81]). Initially, when the charge and the hole are infinitely far apart the total

angular momentum is precisely that of a Thomson dipole (98). As the particle falls radially, the electromagnetic field exerts a torque on the hole, which starts spinning. The initial angular momentum keeps being transferred into the hole until, eventually, the particle crosses the horizon and what is left is a dyonic Kerr–Newman black hole with angular momentum equal to that of the initial Thomson dipole. In other words, one can spin up a non-rotating magnetic black hole by dropping radially an electric particle into it. By returning the geodesic equation of motion 11 one can extend this understanding to the case of spinning KN black holes. This is done by first determining the lorentz force acting on particles along the axis in these spacetimes, which can be found to be given by,

$$u^{\mu}\nabla_{\mu}u^{r} = \frac{e}{m}F^{r}{}_{\nu}u^{\nu} = a\mathcal{L}\frac{2r\Delta(r)}{\left(r^2+a^2\right)^3}u^{t}. \tag{100}$$

Outside the horizon $\Delta(r) > 0$ and a future-directed timelike trajectory has $u^t > 0$, so the force (100) is repulsive or attractive depending on whether a and $\mathcal{L}$ have equal or opposite sign, respectively. It can then be seen that it is this spin-spin repulsion force that causes, a rotating magnetic black hole to tend to accrete charges whose angular momentum differs in sign with that of the hole itself, thus reducing its angular momentum.

In fact, it is also this spin-spin repulsion force that plays a key role in the protection of cosmic censorship in dyonic KN, this can be seen by first considering the extremal case of dyonic KN given by,

$$M^2 = a^2 + P^2 + Q^2. \tag{101}$$

At extremality, for cosmic censorship to be respected, naturally one requires that any perturbations along the KN family of solutions must satisfy, $\delta M \geq \delta(\sqrt{a^2+P^2+Q^2})$, which can be expanded as,

$$(M^2+a^2)\delta M \geq M(Q\delta Q + P\delta P) + a\delta J. \tag{102}$$

Otherwise one would arrive at an over-extremised black hole with a naked singularity.

By considering the conserved quantity relating to the generator of $\mathcal{H}^+$, and recalling that k^a and the 4-velocity of any physical geodesics (u^a) must be causal and future directed, then we have the condition $-mu^a k_a \geq 0$. If we take the conserved energy and angular momentum defined by some geodesic trajectory to be δM and δJ respectively and evaluate the right-hand side of the conserved quantity at $\mathcal{H}^+$. Then through the causal condition, one immediately arrives at 102. Meaning at extremality no causal future-directed geodesic trajectories crossing the horizon exist which can lead to a violation of weak cosmic censorship.

In practice if we restrict to the case of an electrically charged particle in radial motion along the axis of a spinning magnetic black hole. Then there is no centrifugal or direct charge repulsion forces present, in this case it is precisely the electromagnetic spin-spin repulsion force which is protecting cosmic censorship in this context.

7. Penrose Process in dyonic KN

Since its conception [82], the Penrose process has played a prominent role in guiding our intuition when studying dynamical systems involving black holes. In its original and simplest version, it consists in extracting "rotational" energy from the hole by mining the so-called ergoregion, a region in the vicinity of the hole where particles are allowed to be in "negative energy states" relative to asymptotic observers.

At first sight, the Penrose process seems to provide a simple explanation of some high-energy phenomena in which black holes are expected (or known) to be involved, such as active galactic nuclei, relativistic jets and high- and ultra-high-energy cosmic rays. However, it was soon realised [83, 84] that, in order to be a viable process for extracting energy and angular momentum from the hole, the velocities of the decays (or break ups) at the ergoregion need to be in the relativistic regime $v > 1/2$, and in any case the efficiency of the process is bounded to $\lesssim 20\%$. This is true for the mechanical Penrose process, which only involves a neutral rotating black hole. A much different situation arises if the black hole is immersed on an homogeneous magnetic field [11], yielding the so-called magnetised Penrose process, which was first envisaged in [55]. In this case, the resulting electric field (due to the twisting of magnetic field lines induced by the hole's rotation) enhances the Penrose process if the particles resulting from a decay are charged. Assuming that the magnetic field is created by reasonable matter orbiting the hole, the break up velocities in the decay no longer need be relativistic for the magnetised Penrose process to be viable, and efficiencies can be much larger than the aforementioned 20% [54]. However, it is well known that a rotating black hole immersed in an homogeneous magnetic field will accrete a net amount of electric charge, and this turns out to suppress significantly energy extraction [85]. Besides this, the fact that the magnetised Penrose process relies on having a black hole which is not in isolation makes the system quite difficult to model. Alternatively, one could enhance energy extraction while keeping the hole in isolation by allowing it to possess a net amount of electric charge. Unfortunately, in that situation the hole would quickly discharge via Schwinger pair creation [10].

Here we consider endowing the hole with magnetic charge. This is qualitatively different from the cases discussed above, since energy extraction is greatly enhanced (as shown below) while keeping the black hole in isolation, and no discharge mechanism is expected to neutralise the hole since magnetic monopoles are less likely to pair create than electric charges. Of course, as discussed in the introduction the price to pay is the a priori exotic primordial origin of the magnetic charges. In the sake of completeness, we shall derive the main equations for the most general charge configurations first, and then restrict them to the case of a magnetic black hole and electrically charged particles.

The four-velocity of a particle at a given point can be parametrised using $u^r, u^\theta, \mathcal{L}$, while the fourth degree of freedom is fixed using the timelike condition and requiring that the particle's trajectory is future-oriented, which in BL coordinates simply ammounts

to imposing $u^t > 0$.[+] Then, the energy per unit mass is no more a free parameter but a function given by

$$\mathcal{E}(u^r, u^\theta, \mathcal{L}) = -\frac{1}{m}\Omega_{IJ}\mathcal{P}^I_t q^J - \frac{g_{t\phi}}{g_{\phi\phi}}\left(\mathcal{L} - \frac{1}{m}\Omega_{IJ}\mathcal{P}^I_\phi q^J\right) + \sqrt{\frac{\Delta\sin^2\theta}{g_{\phi\phi}}\left(1 + \frac{\left(\mathcal{L} - \frac{1}{m}\Omega_{IJ}\mathcal{P}^I_\phi q^J\right)^2}{g_{\phi\phi}} + g_{rr}(u^r)^2 + g_{\theta\theta}(u^\theta)^2\right)}\,. \tag{103}$$

It is easy to see that outside the event horizon there are states with $\mathcal{E} < 0$ (of course, as in the usual Penrose process, this is not in contradiction with having positive kinetic energy with respect to a local inertial observer). We want to find the regions of spacetime where particles with a given angular momentum $\mathcal{L}$ *can* be in a negative energy state, since it is in those regions where decays or break ups could lead to energy and angular momentum extraction. From (103), it is clear that the minimal energy states are those with $u^r = u^\theta = 0$. So, with that choice, the zero-energy level sets given by (103) enclose the regions where negative energy states are allowed.

Let us focus on the case of an electric particle with charge e and a purely magnetic black hole of charge P, so $Q = g = 0$. We fix the overall scale by setting $M = 1$ and introduce the extremality parameter

$$\epsilon = \sqrt{1 - a^2 - P^2}\,, \tag{104}$$

so $\epsilon = 0$ for extremal black holes and $\epsilon = 1$ for neutral, non-rotating ones. We find negative energy states for values of $\mathcal{L}$ with opposite sign to that of a, similarly to the mechanical Penrose process. There are two regimes of $\mathcal{L}$, defined by the value of the angular momentum of the Thomson dipole (see Figure 9):

- $0 < |\mathcal{L}| < |Pe/m|$: in this regime the presence of the magnetic charge deforms the region of negative energy states by enlarging it along the directions determined by certain conjugate values of the axial angle, θ_0 and $\pi - \theta_0$, with $\theta_0 \in (0, \pi/2)$. θ_0 goes from the equator $\theta_0 = \pi/2$ for $|\mathcal{L}| \approx 0$ (where there are no negative energy states) and approaches the rotation axis $\theta_0 = 0$ as $|\mathcal{L}| \to |Pe/m|$.
- $|\mathcal{L}| = |Pe/m|$: when the angular momentum is precisely that of the Thomson dipole, we find that the region of negative energy states includes the rotation axis. This leads to the quite remarkable possibility of extracting angular momentum (and of course energy) from a hole in a process that is entirely axisymmetric (e.g. a decay happening along the axis). This condition is also the requirement one finds for the existence of motion on the axis.
- $|\mathcal{L}| > |Pe/m|$: in this case we find a similar situation to that of the first regime, where now $\theta_0 \to \pi/2$ as $|\mathcal{L}| \to \infty$, and the region of negative energy states converges

[+] This can be seen by defining the so-called zero angular momentum observer $U = -\frac{dt}{\sqrt{-g^{tt}}}$, which is timelike and future-oriented everywhere outside the hole. The requirement that a timelike trajectory u^μ is also future-oriented is $0 > U_\mu u^\mu = -u^t/\sqrt{-g^{tt}}$.

to the mechanical ergoregion. This is as expected, since for large $\mathcal{L}$ at fixed a, P and e the mechanical effects dominate over the electromagnetic ones.

For all values of $\mathcal{L}$, we notice that the region of negative energy states at the equator $\theta = \pi/2$ is unaffected by P, since the momentum maps vanish there (we recall that in this discussion the electric black hole charge is set to $Q = 0$)

$$\mathcal{P}_t(\theta = \pi/2) = \mathcal{P}_\phi(\theta = \pi/2) = 0\,. \tag{105}$$

On the other hand, for $|\mathcal{L}| = |Pe/m|$ there exist negative energy states along the rotation axis. Such states do not exist in the mechanical case, and furthermore carry angular momentum. Expanding in powers of e/m (which may be motivated by the fact that for an electron $e/m \approx 2 \times 10^{21}$) one finds that the negative energy states along the axis extend up to

$$r_{\rm max} \approx \sqrt{|aPe/m|}\,, \tag{106}$$

which is largest when aP is maximised (as expected since the magnitude of the electric field is roughly given by aP).

For a fixed extremality parameter ϵ, this happens at $a = P = \sqrt{(1-\epsilon^2)/2}$, so for small ϵ one has $a = P \approx 0.707$. The magnification of the region of negative energy states for that choice of parameters can be clearly seen in Figure 9.

We shall also comment on the case that the black hole is endowed not only with magnetic but also electric charge (then the particle can be chosen to be purely electric without loss of generality due to electric magnetic duality). The monopolar electric field enhances the Penrose process and allows both energy and charge extraction even if the black hole is nonrotating. If, in addition, the black hole rotates and possesses magnetic charge the electric field picks a dipolar piece which, in the neighbourhood of one of the components of the rotation axis ($\theta = 0$ or $\theta = \pi$) opposes to the monopolar one. Interestingly, this balance of electric fields leads to the existence of "floating" regions of negative energy states (see Figure 10). That is, after a decay one of the products can reach a negative energy state which is an orbit confined to a neighbourhood of the axis and that never crosses the horizon. Even though that particle never falls into the hole, the other product of the decay can reach infinity and energy is extracted from the system (in such a process there is also extraction of electric charge, but not of angular momentum). Regions of negative energy states that are disconnected from the horizon were also found recently in [85] in the case of rotating magnetised black holes (i.e. rotating black holes immersed in an external magnetic field). Those are toroidal regions centered around the hole and symmetric with respect to the equator, while the ones found here associated to magnetic black holes are simply connected bubble-shaped regions and centered at a point of the axis.

Particles trapped in negative energy regions which are disconnected from the horizon are expected to release more energy via synchrotron radiation, and follow an evolution driven by electromagnetic radiation-reaction [86, 87]. This is a potential topic of interesting future work.

We conclude this section with some remarks about the bounds on the velocity of the break up and the efficiency of the Penrose process. For completeness, we shall do so for the most general charge configuration of both the hole and the particle. A simple computation shows that the specific energy $\mathcal{E}$ of a particle with mass m and charge q^I that is the product of a decay of a particle with specific energy $\mathcal{E}_0$, mass m_0 and charge

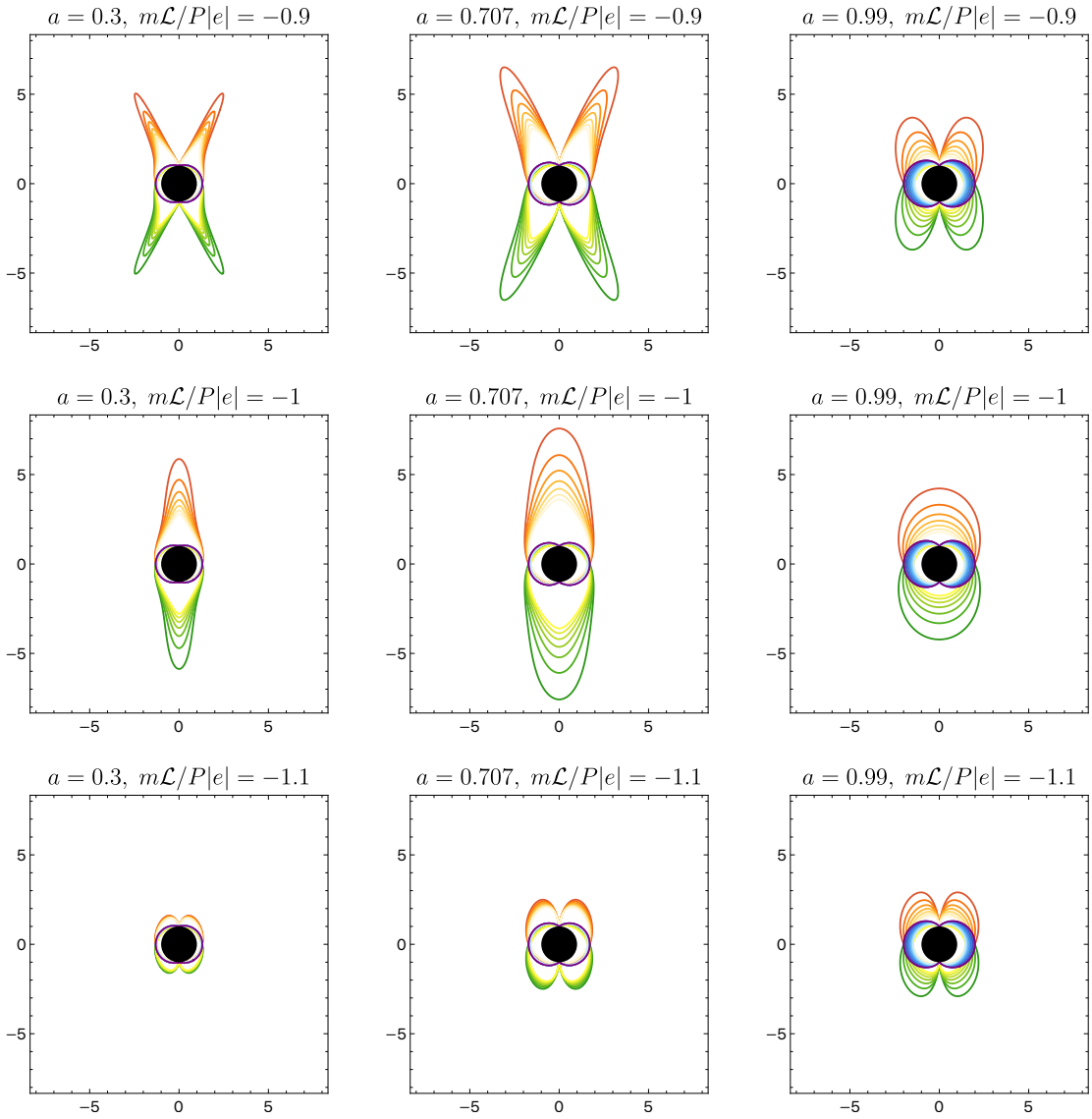

Figure 9. Regions of negative energy states of an electric particle with $e/m = \pm 100$ (red for positive, green for negative) in a rotating magnetic black hole with $M = 1$, $Q = 0$, $\epsilon = 10^{-3}$. The columns correspond to the spin parameters $a = 0.3, 0.707, 0.99$ and the corresponding positive value of magnetic charge P determined by (104), while rows display different values of the particle's angular momentum $m\mathcal{L}/P|e| = -0.9, -1, -1.1$. The contours show the regions of negative energy states given by (103) with $u^r = u^\theta = 0$ (see text). The outermost contour is the zero energy level, and subsequent inner curves decrease by $\Delta\mathcal{E} = -0.5$ the value of the energy level, following the colour scale. In the same conventions, blue contours correspond to a neutral particle, so they are associated to the mechanical Penrose process.

q_0^I must satisfy [55, 84]

$$
\begin{aligned}
&-\frac{1}{m}\Omega_{IJ}\mathcal{P}_t^I q^J+\gamma(v)\left[\mathcal{E}_0+\frac{1}{m_0}\Omega_{IJ}\mathcal{P}_t^I q_0^J-v\sqrt{g_{tt}+\left(\mathcal{E}_0+\frac{1}{m_0}\Omega_{IJ}\mathcal{P}_t^I q_0^J\right)^2}\right]\\
&\leq\mathcal{E}\\
&\leq-\frac{1}{m}\Omega_{IJ}\mathcal{P}_t^I q^J+\gamma(v)\left[\mathcal{E}_0+\frac{1}{m_0}\Omega_{IJ}\mathcal{P}_t^I q_0^J+v\sqrt{g_{tt}+\left(\mathcal{E}_0+\frac{1}{m_0}\Omega_{IJ}\mathcal{P}_t^I q_0^J\right)^2}\right], \quad (107)
\end{aligned}
$$

where v is the absolute value of the velocity of the product in the frame of the decaying particle and $\gamma(v)=1/\sqrt{1-v^2}$ the Lorentz factor. Applying (107) to the decay of a neutral particle into electric charges along the rotation axis of a magnetic black hole, one finds that the lower bound can be negative (and therefore energy extraction is actually possible) only if v satisfies

$$
v>\frac{1-\alpha^2}{1+\alpha^2}\,, \qquad \alpha\equiv\frac{(e/m)aP}{(e_0/m_0)aP+(r_H^2+a^2)\,\mathcal{E}_0}\,. \quad (108)
$$

In particular, v can be arbitrarily close (or equal) to zero if $|\alpha|\geq 1$. This is true for a process taking place along the rotation axis, and similar conclusions can be deduced

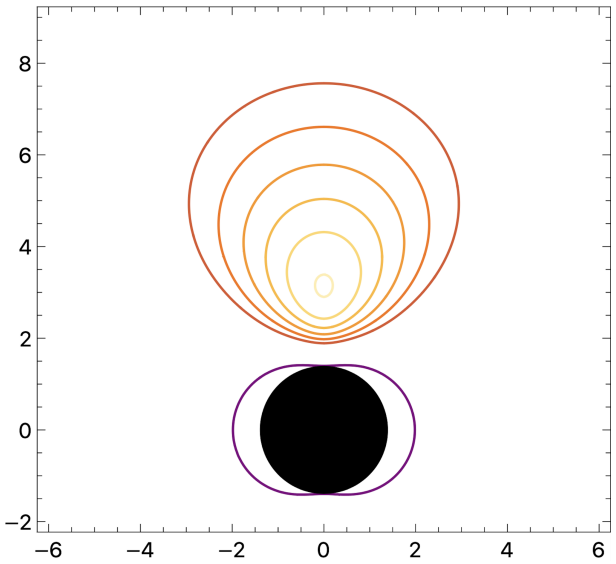

Figure 10. Region of negative energy states for a black hole with parameters $M=1$, $a=0.9$, $Q=-0.085$ and $P=-0.16$. The particle's charge to mass ratio is $e/m=100$ and its angular momentum per unit mass is $\mathcal{L}=-Pe/m=16$. The outermost red contour corresponds to the zero-energy surface and the successive inner ones decrease the energy by -0.1, following the color scale. The purple contour is the mechanical ergosurface. As explained in the text, the attractive gravitational and coulomb forces are compensated by the repulsive dipolar force, thus leading to disconnected regions of negative energy states.

for processes in the enlarged regions of negative energy states. As noted above, one exception are processes happening at the equator $\theta = \pi/2$, where (105) holds and the bounds on v are the same as in the mechanical Penrose process. Similarly, it is easy to see from (103) and (107) that the efficiency of energy extraction $\eta \equiv (m\mathcal{E} - m_0\mathcal{E}_0)/m_0\mathcal{E}_0$ can be made significantly larger than that of the mechanical Penrose process for decays happening off the equator, while at the equator the bounds on the efficiency remain the same.

Finally, we remark that similarly to the mechanical Penrose process the amount of energy that can be extracted from the hole is bounded by the irreducible mass, defined as $M_{IRR}^2 = A_H/16\pi = (a^2 + r_H^2)/4$ where A_H is the area of a spatial section of the horizon. Indeed, in a Penrose process involving the decay of a charged particle one has $\delta M_{IRR} \geq 0$ (in agreement with the second law of black hole mechanics). At the same time,

$$M^2 = \left(M_{IRR} + \frac{P^2 + Q^2}{4M_{IRR}}\right)^2 + \frac{J^2}{4M_{IRR}^2} \geq M_{IRR}^2, \tag{109}$$

so the amount of energy that can be extracted from the hole is necessarily smaller than $M - M_{IRR}$.

8. Discussion

The work in this thesis has provided a comprehensive analysis and many novel extensions to the understanding of test particle motion in Kerr and dyonic KN spacetimes. In the first half of this work which focused on the uncharged Kerr solution, we have solved for the closed-form analytic solutions to generic bound plunging geodesics in Kerr. We have also paid particular attention to the special cases of plunges starting asymptotically from the innermost stable processing circular orbit and from unstable spherical orbits, in which the solutions take a particularly simple form. This generalises the result of [42, 74] to inclined motion. The general expression for the inflow in this case, is more involved due to oscillations coming from the polar motion. Therefore we have provided two simplified approximations for the inflow rate. We have also found that the geodesics asymptoting from the ISSO can be parametrised purely in terms of black hole spin and the radius of the ISSO. We expect these solutions to have applications in the modeling of accretion flow in Kerr spacetimes. In addition to the special case of ISSO plunges.

We expect the provided generic solutions for plunging geodesics to find practical use in modeling the inspiral of binary black holes since in the small mass-ratio limit they will describe the final phase of the inspiral before merger. As small mass-ratio methods are applied to more equal mass systems, including this phase becomes increasingly important. For ease of application, we have incorporated our results in the `KerrGeodesics` package in the Black hole perturbation toolkit [3]. We are aware of multiple members of the self-force community who are already making use of these results and packages we have provided.

In the second half of this thesis, we reinstate the charge parameters $\{e, q, Q, P\}$

and analyse in depth the little-studied phenomenology which can occur in these dyonic KN configurations. In particular, we study in detail how a particle in radial motion along the rotation axis actually acquires a non-zero angular momentum. We also show how this contribution to the angular momentum leads to the existence of a spin-spin repulsion force which acts to lower the spin of the hole when immersed in an ionised medium. Additionally, we also analyse in depth the modified Penrose process which occurs in dyonic KN, showing the existence of bubble-shaped ergoregions disconnected from the hole and providing a novel understanding of the scaling of these regions with respect to spin and angular momentum at fixed extremalities. Finally, we have also developed a `package` implementing our generic solutions to bound and plunging motion in dyonic KN in terms of Jacobi elliptic functions.

References

[1] C. Dyson and M. van de Meent, Kerr-fully Diving into the Abyss: Analytic Solutions to Plunging Geodesics in Kerr, (2023), arXiv:2302.03704 [gr-qc].

[2] C. Dyson and D. Pereñiguez, Magnetic Black Holes: from Thomson Dipoles to the Penrose Process and Cosmic Censorship, (2023), arXiv:2306.15751 [gr-qc].

[3] Black Hole Perturbation Toolkit, (bhptoolkit.org).

[4] R. P. Kerr, Gravitational field of a spinning mass as an example of algebraically special metrics, Phys. Rev. Lett. **11**, 237 (1963).

[5] E. T. Newman, E. Couch, K. Chinnapared, A. Exton, A. Prakash, and R. Torrence, Metric of a Rotating, Charged Mass, Journal of Mathematical Physics **6**, 918 (1965).

[6] B. Carter, Axisymmetric Black Hole Has Only Two Degrees of Freedom, Phys. Rev. Lett. **26**, 331 (1971).

[7] D. C. Robinson, Uniqueness of the kerr black hole, Phys. Rev. Lett. **34**, 905 (1975).

[8] R. Ruffini and J. A. Wheeler, Introducing the black hole, Phys. Today **24**, 30 (1971).

[9] S. W. Hawking and G. F. R. Ellis, The Large Scale Structure of Space-Time, Cambridge Monographs on Mathematical Physics (Cambridge University Press, 2011).

[10] G. W. Gibbons, Vacuum Polarization and the Spontaneous Loss of Charge by Black Holes, Commun. Math. Phys. **44**, 245 (1975).

[11] R. M. Wald, Black hole in a uniform magnetic field, Phys. Rev. D **10**, 1680 (1974).

[12] V. S. Beskin and I. V. Kuznetsova, On the blandford - znajek mechanism of the energy loss of a rotating black hole, Nuovo Cim. B **115**, 795 (2000), arXiv:astro-ph/0004021.

[13] C. Palenzuela, C. Bona, L. Lehner, and O. Reula, Robustness of the Blandford-Znajek mechanism, Class. Quant. Grav. **28**, 134007 (2011), arXiv:1102.3663 [astro-ph.HE].

[14] F. J. Zerilli, Perturbation analysis for gravitational and electromagnetic radiation in a reissner-nordstroem geometry, Phys. Rev. D **9**, 860 (1974).

[15] M. Johnston, R. Ruffini, and F. Zerilli, Electromagnetically induced gravitational radiation, Phys. Lett. B **49**, 185 (1974).

[16] V. Moncrief, Stability of reissner-nordström black holes, Phys. Rev. D **10**, 1057 (1974).

[17] U. H. Gerlach and U. K. Sengupta, GAUGE INVARIANT PERTURBATIONS ON MOST GENERAL SPHERICALLY SYMMETRIC SPACE-TIMES, Phys. Rev. D **19**, 2268 (1979).

[18] U. H. Gerlach and U. K. Sengupta, GAUGE INVARIANT COUPLED GRAVITATIONAL, ACOUSTICAL, AND ELECTROMAGNETIC MODES ON MOST GENERAL SPHERICAL SPACE-TIMES, Phys. Rev. D **22**, 1300 (1980).

[19] S. Chandrasekhar and B. C. Xanthopoulos, On the metric perturbations of the reissner–nordström black hole, Proceedings of the Royal Society of London. A. Mathematical and Physical Sciences **367**, 1 (1979).

[20] G. Carullo, D. Laghi, N. K. Johnson-McDaniel, W. Del Pozzo, O. J. C. Dias, M. Godazgar, and J. E. Santos, Constraints on Kerr-Newman black holes from merger-ringdown gravitational-wave observations, Phys. Rev. D **105**, 062009 (2022), arXiv:2109.13961 [gr-qc].

[21] O. J. C. Dias, M. Godazgar, J. E. Santos, G. Carullo, W. Del Pozzo, and D. Laghi, Eigenvalue repulsions in the quasinormal spectra of the Kerr-Newman black hole, Phys. Rev. D **105**, 084044 (2022), arXiv:2109.13949 [gr-qc].

[22] A. De Rujula, S. L. Glashow, and U. Sarid, CHARGED DARK MATTER, Nucl. Phys. **B333**, 173 (1990).

[23] M. L. Perl and E. R. Lee, The search for elementary particles with fractional electric charge and the philosophy of speculative experiments, Am. J. Phys. **65**, 698 (1997).

[24] B. Holdom, Two U(1)'s and Epsilon Charge Shifts, Phys. Lett. **B166**, 196 (1986).

[25] K. Sigurdson, M. Doran, A. Kurylov, R. R. Caldwell, and M. Kamionkowski, Dark-matter electric and magnetic dipole moments, Phys. Rev. **D70**, 083501 (2004), [Erratum: Phys. Rev.D73,089903(2006)], arXiv:astro-ph/0406355 [astro-ph].

[26] S. Davidson, S. Hannestad, and G. Raffelt, Updated bounds on millicharged particles, JHEP **05**, 003, arXiv:hep-ph/0001179.

[27] S. D. McDermott, H.-B. Yu, and K. M. Zurek, Turning off the Lights: How Dark is Dark Matter?, Phys. Rev. D **83**, 063509 (2011), arXiv:1011.2907 [hep-ph].

[28] V. Cardoso, C. F. B. Macedo, P. Pani, and V. Ferrari, Black holes and gravitational waves in models of minicharged dark matter, JCAP **05**, 054, [Erratum: JCAP 04, E01 (2020)], arXiv:1604.07845 [hep-ph].

[29] M. Khalil, N. Sennett, J. Steinhoff, J. Vines, and A. Buonanno, Hairy binary black holes in Einstein-Maxwell-dilaton theory and their effective-one-body description, Phys. Rev. D **98**, 104010 (2018), arXiv:1809.03109 [gr-qc].

[30] Y. Bai and N. Orlofsky, Primordial Extremal Black Holes as Dark Matter, Phys. Rev. D **101**, 055006 (2020), arXiv:1906.04858 [hep-ph].

[31] P. K. Gupta, T. F. M. Spieksma, P. T. H. Pang, G. Koekoek, and C. V. D. Broeck, Bounding dark charges on binary black holes using gravitational waves, Phys. Rev. D **104**, 063041 (2021), arXiv:2107.12111 [gr-qc].

[32] K. Kritos and J. Silk, Mergers of maximally charged primordial black holes, Phys. Rev. D **105**, 063011 (2022), arXiv:2109.09769 [gr-qc].

[33] B. Carter, Global structure of the Kerr family of gravitational fields, Phys. Rev. **174**, 1559 (1968).

[34] S. Chandrasekhar, The mathematical theory of black holes, Oxford classic texts in the physical sciences (Oxford Univ. Press, Oxford, 2002).

[35] D. C. Wilkins, Bound Geodesics in the Kerr Metric, Phys. Rev. D **5**, 814 (1972).

[36] G. V. Kraniotis, Precise relativistic orbits in Kerr space-time with a cosmological constant, Class. Quant. Grav. **21**, 4743 (2004), arXiv:gr-qc/0405095.

[37] Y. Mino, Perturbative approach to an orbital evolution around a supermassive black hole, Phys. Rev. D **67**, 084027 (2003), arXiv:gr-qc/0302075.

[38] R. Fujita and W. Hikida, Analytical solutions of bound timelike geodesic orbits in Kerr spacetime, Class. Quant. Grav. **26**, 135002 (2009), arXiv:0906.1420 [gr-qc].

[39] M. van de Meent, Analytic solutions for parallel transport along generic bound geodesics in Kerr spacetime, Class. Quant. Grav. **37**, 145007 (2020), arXiv:1906.05090 [gr-qc].

[40] E. Hackmann and H. Xu, Charged particle motion in Kerr-Newmann space-times, Phys. Rev. D **87**, 124030 (2013), arXiv:1304.2142 [gr-qc].

[41] E. Hackmann, C. Lammerzahl, V. Kagramanova, and J. Kunz, Analytical solution of the geodesic equation in Kerr-(anti) de Sitter space-times, Phys. Rev. D **81**, 044020 (2010), arXiv:1009.6117 [gr-qc].

[42] A. Mummery and S. Balbus, Inspirals from the Innermost Stable Circular Orbit of Kerr Black Holes: Exact Solutions and Universal Radial Flow, Phys. Rev. Lett. **129**, 161101 (2022), arXiv:2209.03579 [gr-qc].

[43] L. Barack and A. Pound, Self-force and radiation reaction in general relativity, Rept. Prog. Phys. **82**, 016904 (2019), arXiv:1805.10385 [gr-qc].

[44] T. Hinderer and E. E. Flanagan, Two timescale analysis of extreme mass ratio inspirals in Kerr. I. Orbital Motion, Phys. Rev. D **78**, 064028 (2008), arXiv:0805.3337 [gr-qc].

[45] A. Pound and B. Wardell, Black hole perturbation theory and gravitational self-force 10.1007/978-981-15-4702-7-38-1 (2021), arXiv:2101.04592 [gr-qc].

[46] J. Miller and A. Pound, Two-timescale evolution of extreme-mass-ratio inspirals: waveform generation scheme for quasicircular orbits in Schwarzschild spacetime, Phys. Rev. D **103**, 064048 (2021), arXiv:2006.11263 [gr-qc].

[47] S. Hadar and B. Kol, Post-ISCO Ringdown Amplitudes in Extreme Mass Ratio Inspiral, Phys. Rev. D **84**, 044019 (2011), arXiv:0911.3899 [gr-qc].

[48] G. d'Ambrosi and J. W. van Holten, Ballistic orbits in Schwarzschild space-time and gravitational waves from EMR binary mergers, Class. Quant. Grav. **32**, 015012 (2015), arXiv:1406.4282 [gr-qc].

[49] G. Compère and L. Küchler, Asymptotically matched quasi-circular inspiral and transition-to-plunge in the small mass ratio expansion, SciPost Phys. **13**, 043 (2022), arXiv:2112.02114 [gr-qc].
[50] A. Apte and S. A. Hughes, Exciting black hole modes via misaligned coalescences: I. Inspiral, transition, and plunge trajectories using a generalized Ori-Thorne procedure, Phys. Rev. D **100**, 084031 (2019), arXiv:1901.05901 [gr-qc].
[51] O. Burke, J. R. Gair, and J. Simón, Transition from Inspiral to Plunge: A Complete Near-Extremal Trajectory and Associated Waveform, Phys. Rev. D **101**, 064026 (2020), arXiv:1909.12846 [gr-qc].
[52] G. Compère, K. Fransen, and C. Jonas, Transition from inspiral to plunge into a highly spinning black hole, Class. Quant. Grav. **37**, 095013 (2020), arXiv:1909.12848 [gr-qc].
[53] G. Compère and L. Küchler, Self-consistent adiabatic inspiral and transition motion, Phys. Rev. Lett. **126**, 241106 (2021), arXiv:2102.12747 [gr-qc].
[54] A. Tursunov and N. Dadhich, Fifty years of energy extraction from rotating black hole: revisiting magnetic Penrose process, Universe **5**, 125 (2019), arXiv:1905.05321 [astro-ph.HE].
[55] S. M. Wagh, S. V. Dhurandhar, and N. Dadhich, Revival of penrose process for astrophysical applications, Atrophys. J. **301**, 1018 (1986).
[56] F. J. Ernst, Black holes in a magnetic universe, J. Math. Phys. **17**, 54 (1976).
[57] F. J. Ernst and W. J. Wild, Kerr black holes in a magnetic universe, Journal of Mathematical Physics **17**, 182 (1976).
[58] S. W. Hawking and G. F. R. Ellis, The Large Scale Structure of Space-Time, Cambridge Monographs on Mathematical Physics (Cambridge University Press, 1973).
[59] B. Carter, Black holes equilibrium states, in Les Houches Summer School of Theoretical Physics: Black Holes (1973) pp. 57–214.
[60] S. Grunau and V. Kagramanova, Geodesics of electrically and magnetically charged test particles in the Reissner-Nordström space-time: analytical solutions, Phys. Rev. D **83**, 044009 (2011), arXiv:1011.5399 [gr-qc].
[61] T. Ortin, Gravity and Strings, 2nd ed., Cambridge Monographs on Mathematical Physics (Cambridge University Press, 2015).
[62] Z. Elgood, P. Meessen, and T. Ortín, The first law of black hole mechanics in the Einstein-Maxwell theory revisited, JHEP **09**, 026, arXiv:2006.02792 [hep-th].
[63] T. Ortin and D. Pereñiguez, Magnetic charges and Wald entropy, JHEP **11**, 081, arXiv:2207.12008 [hep-th].
[64] P. Stäckel, Ueber die bewegung eines punktes in einer n-fachen mannigfaltigkeit., Mathematische Annalen **41**, 537 (1893).
[65] B. Carter, Global structure of the kerr family of gravitational fields, Phys. Rev. **174**, 1559 (1968).
[66] M. Walker and R. Penrose, On quadratic first integrals of the geodesic equations for type [22] spacetimes, Commun. Math. Phys. **18**, 265 (1970).
[67] W. Kinnersley, Type D Vacuum Metrics, J. Math. Phys. **10**, 1195 (1969).
[68] S. E. Gralla and A. Lupsasca, Null geodesics of the Kerr exterior, Phys. Rev. D **101**, 044032 (2020), arXiv:1910.12881 [gr-qc].
[69] J. M. Bardeen, Timelike and null geodesics in the Kerr metric, Proceedings, Ecole d'Eté de Physique Théorique: Les Astres Occlus : Les Houches, France, August, 1972, 215-240 , 215 (1973).
[70] S. Drasco and S. A. Hughes, Gravitational wave snapshots of generic extreme mass ratio inspirals, Phys. Rev. D **73**, 024027 (2006), [Erratum: Phys.Rev.D 88, 109905 (2013), Erratum: Phys.Rev.D 90, 109905 (2014)], arXiv:gr-qc/0509101.
[71] E. Teo, Spherical orbits around a Kerr black hole, Gen. Rel. Grav. **53**, 10 (2021), arXiv:2007.04022 [gr-qc].
[72] G. Compère and A. Druart, Near-horizon geodesics of high-spin black holes, Phys. Rev. D **101**, 084042 (2020), [Erratum: Phys.Rev.D 102, 029901 (2020)], arXiv:2001.03478 [gr-qc].
[73] L. C. Stein and N. Warburton, Location of the last stable orbit in Kerr spacetime, Phys. Rev. D

101, 064007 (2020), arXiv:1912.07609 [gr-qc].
[74] A. Mummery and S. Balbus, A complete characterisation of the orbital shapes of the non-circular Kerr geodesic solutions with circular orbit constants of motion, (2023), arXiv:2302.01159 [gr-qc].
[75] G. Labahn and M. Mutrie, Reduction of elliptic integrals to legendre normal form, (1997).
[76] J. J. Thomson, Elements of the Mathematical Theory of Electricity and Magnetism, 4th ed., Cambridge Library Collection - Mathematics (Cambridge University Press, 2009).
[77] M. N. Saha, Note on dirac's theory of magnetic poles, Phys. Rev. **75**, 1968 (1949).
[78] H. A. Wilson, Note on dirac's theory of magnetic poles, Phys. Rev. **75**, 309 (1949).
[79] D. Garfinkle and S.-J. Rey, Angular momentum of an electric charge and magnetically charged black hole, Phys. Lett. B **257**, 158 (1991).
[80] C. Bunster and M. Henneaux, A Monopole Near a Black Hole, (2007), arXiv:hep-th/0703155.
[81] J. H. Kim and S.-H. Moon, Electric Charge in Interaction with Magnetically Charged Black Holes, JHEP **09**, 088, arXiv:0707.4183 [gr-qc].
[82] R. Penrose, Gravitational collapse: The role of general relativity, Riv. Nuovo Cim. **1**, 252 (1969).
[83] J. M. Bardeen, W. H. Press, and S. A. Teukolsky, Rotating Black Holes: Locally Nonrotating Frames, Energy Extraction, and Scalar Synchrotron Radiation, Astrophys. J. **178**, 347 (1972).
[84] R. M. Wald, Energy Limits on the Penrose Process, Astrophys. J. **191**, 231 (1974).
[85] K. Gupta, Y. T. A. Law, and J. Levin, Penrose process for a charged black hole in a uniform magnetic field, Phys. Rev. D **104**, 084059 (2021), arXiv:2106.15010 [gr-qc].
[86] J. a. S. Santos, V. Cardoso, and J. Natário, Electromagnetic radiation reaction and energy extraction from black holes: The tail term cannot be ignored, Phys. Rev. D **107**, 064046 (2023), arXiv:2303.03411 [gr-qc].
[87] N. P. Baker and V. P. Frolov, Charged Particle Motion Near a Magnetized Black Hole: A Near-Horizon Approximation, (2023), arXiv:2305.12591 [gr-qc]